MSc in Environmental Engineering

Faculty of Civil Engineering and Geosciences

Concentrating hemicellulosic hydrolysates with different membrane technologies

A study on dewatering C5/C6 sugar streams with Nanofiltration and Membrane Distillation.

Anastasia Saranti

MSc Thesis, 2021

TU Delft

CONCENTRATING HEMICELLULOSIC HYDROLYSATES WITH DIFFERENT MEMBRANE TECHNOLOGIES

A study on dewatering C5/C6 sugar streams with Nanofiltration and Membrane Distillation.

A thesis submitted to the Delft University of Technology in partial fulfillment of the requirements for the degree of
Master of Science in Civil Engineering

To be defended publicly on July 8^{th}, 2021 at 9:00 AM.

by

Anastasia Saranti

Chair and supervisor :	Dr. Ir. S.G.J. Heijman
Supervisor :	Dr. Ir. Henri Spanjers
Supervisor :	Dr. Ir. Ralph Lindeboom
Company supervisor :	Ir. N. van Linden

TU Delft IMPRESS LENNTECH Water Treatment Solutions

ACKNOWLEDGEMENTS

This MSc thesis completes my academic journey in TU Delft. Although this report denotes the end of an era, the things I have learned and experienced throughout this journey have created new worlds for me to discover. Several people have contributed to the completion of this work.

First of all, I would like to thank David van Lennep for giving me the opportunity to conduct my MSc thesis research in Lenntech and for helping me get involved in the "IMPRESS" project. I gained so much from being in Lenntech's R&D team and especially, from working under the supervision of Niels van Linden. Niels, I would like to express my greatest appreciation for your help during this year. Thank you for always trying to find time to provide me with feedback, for sharing your perspective on different things and for encouraging me throughout the (totally unpredictable) lab experiments. I would like to extend my sincere thanks to the whole R&D team in Lenntech for the nice time and the great conversations we had.

I would also like to express my deepest gratitude to my committee members: Dr. Ir. Bas Heijman, Dr. Ir. Henri Spanjers and Dr. Ir. Ralph Lindeboom. Your insightful comments and critical feedback were an enormous help to me and guided me to discover new scientific aspects in this research and obtain a more holistic view of the project. I would also like to acknowledge the assistance of Jolanda van Haagen and Agnieszka Kooijman in the analysis of my samples.

The completion of this thesis would not have been possible without the support of those special people. To the international family I got in Delft and to those friends that are always close (regardless of the distance), thank you all for your relentless support, the amazing moments and the endless conversations. Finally, I want to thank my family for their unconditional love and understanding. Your sacrifices all these years, our extended online "consultation" hours and your big smiles remind me how truly privileged I am to have you by my side.

ABSTRACT

This thesis constitutes a part of the "IMPRESS" project which is aiming at the production of bio-plastics by utilizing hemicellulosic hydrolysates. The hydrolysate stream, after following the steps of acid hydrolysis and neutralization, consists of monosaccharides (C5/C6 sugars), salt and sugar degradation products. The C5/C6 sugars need to be concentrated by a factor of 10 to be purified afterwards in downstream processes. Evaporation has been the most dominant technology in the sugar treatment sector, however the current study aimed to investigate tubular nanofiltration (NF) and vacuum membrane distillation (VMD) units for concentrating the C5/C6 sugars, as more sustainable alternatives. Synthetic solutions with C5/C6 sugars and salt were used to assess the performance of the NF and MD membranes in terms of sugar and salt rejection before the experiments with the real hydrolysate solution. Among the different NF and MD membranes, the one that met the C5/C6 sugar rejection requirements (>90%) during the synthetic solution experiments was tested for concentrating the C5/C6 sugars. The most suitable technology for concentrating the C5/C6 sugars was also assessed for its energy consumption. Additionally, single filtration tests were conducted to characterize the NF membranes, while surface tension and contact angle measurements were performed to predict the membrane wetting phenomena during the VMD operation.

Based on the C5/C6 sugar rejection values (range of 22-81%) obtained with ceramic and polymeric NF membranes, it was deduced that the tubular NF membranes were not capable of meeting the C5/C6 sugar concentration goals. The polymeric membranes performed better than the ceramic ones in terms of C5/C6 sugar rejection, with a maximum sugar rejection of 81%. However, the polymeric membranes were found to be more prone to fouling, showing a maximum decrease of 34 % in the water permeability after 4 hours of operation with the hydrolysate solution. Additionally, the characterization of the NF membranes based on the Donnan Steric Pore Model (DSPM) revealed membrane pore sizes larger than those provided by the manufacturer. On the contrary, the 0.2 μm MD membrane showed >99 % of C5/C6 sugar rejection and was used for the sugar concentration tests. The maximum C5/C6 sugar concentration factor (CF) achieved with the VMD was 8 with a negligible sugar loss (<1%) in the permeate, indicating that concentrating the C5/C6 sugars by a factor of 10 is feasible with this technology. Surface tension and contact angle measurements disclosed inconsistencies in the hydrophobicity of the MD membrane, which can be linked to the membrane wetting phenomena occurred during the VMD operation. The fouling of the MD membrane (50 % of flux decrease after 39 hours of operation) was found to be reversible with complete flux recovery after chemical cleaning and drying of the membrane.

The energy assessment of the VMD technology showed that the main energy consumer was the cooler, contributing to 96 % of the total consumed energy. Based on the cooler's efficiency, the energy consumption of the VMD unit was calculated to be in the range of 207-736 KWh/m^3 of distillate. When compared with multi-effect evaporators with up to three effects, the VMD was found to be more energy efficient. Investigating less energy-intensive alternatives for concentrating the C5/C6 sugars, experiments with electrodialysis (ED) showed 90% removal of both acid and salt from the raw and neutralized hydrolysate water, respectively, making it feasible for reverse osmosis (RO) membranes to be further tested for concentrating the C5/C6 sugars. Therefore, a treatment scheme of ED and tubular RO membranes is proposed for further research on concentrating the C5/C6 sugars. Overall, a pre-treatment step with the most permeable ceramic NF membrane is suggested, as evinced by the high color removal achieved (elimination of big foulants) and the high permeation of the C5/C6 sugars and salt.

CONTENTS

LIST OF FIGURES

LIST OF TABLES

ACRONYMS

NOMENCLATURE

Greek Symbols

β	geometric factor for the membrane pores [-]
ΔP	net pressure difference [Pa]
ΔP_f	pressure drop due to friction [Pa]
δ_m	membrane thickness [mm]
ϵ_{pl}	efficiency of feed pump [-]
ϵ_{pl}	isentropic efficiency of vacuum pump [-]
η_c	percentage of non-condensable gases [%]
η_s	efficiency of feed pump [-]
γ_l	liquid's surface tension [mN/m]
γ_s	solid's surface tension [mN/m]
λ	latent heat of vaporisation [KJ/kg]
λ_i	ratio of solute radius to pore radius [-]
ϕ	fugacity [-]
Φ_i	steric coefficient [-]
θ	liquid's contact angle [^{o}]

Superscripts

d	dispersive
p	polar

Other Symbols

A	membrane area [cm^2]
C_f	concentration of solute in the feed [% wt]
C_p	concentration of solute in permeate [%wt]
$C_{p,g}$	heat capacity of water vapor [kJ/kg/K]
$D_{i,\infty}$	diffusion coefficient of the solute in the bulk [m^2/s]
$D_{i,pore}$	diffusion coefficient of the solute inside the pore [m^2/s]
j_s	solute flux [mol/(m^2s)
J_v	water flux [L/m^2/h] or [LMH]
k	isentropic exponent [-]
$K_{i,c}$	hindered convective mass transfer coefficient [-]
$K_{i,d}$	hindered diffusive mass transfer coefficient [-]
m_p	mass flow rate of permeate [kg/s]

N	number of evaporator-effects
P_s	isentropic power of the vacuum pump [kW]
$P_{i,f}$	partial feed vapor pressure [Pa]
Pe_i	Peclet number [-]
$q_{V,in}$	volumetric gas flow rate [m^3/s]
R	universal gas constant [J/K/mol]
R_i	solute rejection [-]
r_o	observed solute rejection [-]
r_p	pore radius [nm]
R_w	water recovery [-]
R_{lim}	limiting rejection [-]
T	temperature [^{o}C]
t	time [hr]
V_f	volumetric feed flow rate [m^3/s]

Subscripts

atm	atmospheric
$calc$	calculated
exp	experimental
f	feed
in	inlet
l	liquid
lim	limiting
out	outlet
p	permeate
s	solid
tot	total

1 INTRODUCTION

1.1 BACKGROUND INFORMATION

The need for sustainability in the energy & production field has led to the emergence of bio-refineries. The operation of a bio-refinery is equivalent to that of a petroleum refinery, but instead of using fossil fuels, renewable sources are used as raw materials [Brodin et al., 2017]. Bio-refineries utilize biomass that is destined to be converted into useful bio-products, such as plastics and fuels. The lignocellulosic biomass can be used as a renewable source in order for fossil fuels to be replaced during production. Lignocellulosic biomass originates mainly from agricultural and forest residues and consists of polymeric carbohydrates, such as cellulose and hemicellulose, along with lignin [De Bhowmick et al., 2018]. More specifically, the lignocellulosic biomass that is derived from plants consists of approximately 20-35% hemicellulose, 35-50% cellulose and 10-25% lignin [Brodin et al., 2017].

Following a suitable treatment, lignocellulosic biomass can be converted into sugars and lignin [Galbe and Wallberg, 2019]. Acid hydrolysis is a very common pre-treatment step in order to obtain the different lignocellulosic fractions [Maiti et al., 2012]. During hydrolysis, hemicellulose can yield xylose and glucose among other monomeric sugars [De Bhowmick et al., 2018]. Depending on the type of the biomass source that is used, e.g. softwood, hardwood or grass, different hemicellulose and lignin fragments can be derived. Regarding the hemicellulose, the hydro-carbonate fractions of xylose and glucose are referred as C5 and C6 sugars, respectively, indicating the number of carbon atoms in their structure [Käldström et al., 2014], [De Bhowmick et al., 2018]. After hydrolysis, the aforementioned sugar constituents can be used in the food industry for the production of bio-materials, of polymers and resins [Galbe and Wallberg, 2019]. The chemicals that can be produced from the hemicellulosic biomass, such as xylitol, can be then used as materials in coatings, pharmaceuticals and in the paper-making industry [Peng et al., 2019]. Another chemical that can be produced from wood-based feed-stocks is bio-ethylene, which apart from being a very important monomer used in the composition of plastic, it can also be used for the production of other valuable monomers, such as propylene and ethylene glycol. The latter can be used for the production of bio-plastics, equivalent to fossil-fuel based polyethylene terephthalate (PET) and polyethylene naphthalate (PEN) plastics [Brodin et al., 2017]. With an acid pretreatment of lignocelluloses, the final hydrolysate solution becomes very acidic and thus, the increase of pH is necessary to be able to perform further downstream processes with the hydrolysates, like the one of fermentation [Maiti et al., 2012]. Besides the very acidic water, the acid hydrolysis leads to the production of several impurities from the lignocellulosic biomass, such as acetic and formic acid, furfural and hydroxymethylfurfural (HMF) , that can have a negative effect in the downstream processes [Dey et al., 2020].

Since September 2019, Avantium has been coordinating the "IMPRESS" project, whose main objective is the utilisation of non-edible biomass aiming at renewable chemicals' production. The main goal of the project is to develop and upscale separation and purification procedures, in order to obtain sugar-based monomer ethylene glycol (MEG) and monomer propylene glycol (MPG). The products need to meet the requirements for sustainability and the integrated system is expected to minimise the capital costs (CAPEX) and operational costs (OPEX). The first step in the process scheme includes the acid

hydrolysis of the lignocellulosic biomass in two steps, with the addition of hydrochloric acid (HCl) and the production of crude lignin and C5/C6 sugars. The aforementioned products will be further purified with appropriate technologies to obtain the desirable final products. The composition of the hydrolysate from Avantium can be analyzed to 1 wt % C5/C6 sugars and 0.5 wt % sugar degradation products. Along with the monomeric sugars and sugar degradation products, the hydrolysate water also contains 1.6 wt % of inorganic ions as a result of the stream's neutralization. To achieve the purification goals, the sugar hydrolysates need to be primarily concentrated. The impurities originating from the hydrolysis, like the sugar degradation products, should preferably be reduced as much as possible. Considering the evaporation process as the most dominant and energy intensive one with the purpose of concentrating sugars [Zhang et al., 2020], the current research is focusing on membrane filtration by investigating more sustainable alternatives for this matter.

1.2 TECHNOLOGIES IN SUGAR TREATMENT

Sugar processing has been considered challenging, not only because of the amount of energy that is required but also because of the difficulty in selecting the most suitable membrane technology for the purpose of treating sugars [Rafik et al., 2015]. Regarding the application of membrane technologies for concentrating sugars, the challenges mainly concern the highly polluted streams, which are usually highly viscous and therefore, require high osmotic pressure during their treatment [Hinkova et al., 2002]. There have been many studies on concentrating sugars using pressure driven membranes such as ultrafiltration (UF), nanofiltration (NF) and reverse osmosis (RO). Research has also been done on different membrane materials other than polymeric, such as ceramic [Trägårdh and Gekas, 1988], [Hinkova et al., 2002],[Jiao et al., 2004], [Galbe and Wallberg, 2019] and for different membrane configurations like the one of tubular membrane modules [Doherty et al., 2010],[Chong and Wang, 2019]. Additionally, thermally driven processes have also been studied in the field of sugar treatment, such as the membrane distillation (MD) technology. Different literature findings about sugar recovery through membrane distillation indicate that, MD can improve the product's quality and reduce the energy consumption during treatment [Jiao et al., 2004],[Madhumala et al., 2014], [Liu et al., 2016], [Intan Shafinas Muhammad and A Rosentrater, 2020].

The application of NF and RO membranes in sugar recovery has been widely studied. Early studies have shown that the NF technology is a suitable technology for concentrating sugars [Hinkova et al., 2002], [Amidon and Liu, 2009]. More specifically, the study from Amidon and Liu, showed that xylose can be concentrated by a factor of 2.5 with a NF membrane, while almost all the sugar degradation products can pass in the permeate stream. Additionally, in more recent studies by Gautam and Menkhaus and Ajao et al., both RO and NF membranes have been proven to be suitable for concentrating lignocellulosic hydrolysates. In the study by Gautam and Menkhaus, the different C5/C6 sugars were concentrated with RO and NF by a concentration factor in a range of 2.3-3, showing however irreversible membrane fouling. A similar concentration factor for C5 sugars was achieved with spiral wound RO membranes in the study by Ajao et al.. Even though that NF and RO membranes seem to be more preferable in the sugar concentration field, due to their energy efficiency, the major challenge of their application lies in the membrane fouling [Zhang et al., 2020]. The findings of Vellenga and Trägårdh support those of Zhang et al., regarding the severe fouling phenomena of the NF membranes during sugar processing. However, more recent studies like the one by Maiti et al. have shown that flat sheet and spiral wound NF membranes yield promising results for concentrating hydrolysates showing insignificant membrane fouling. Additionally, the study by Ajao et al. has shown that the fouling can be reversible for spiral wound RO membranes in the case of hydrolysate treatment.

The use of thin film polyamide NF membranes is imperative among the food and paper industry. For hydrolysed streams that are being neutralized, the influence of salts as a neutralization product has been widely studied in sugar recovery processes using polyamide flat-sheet NF membranes. NF membranes are proven to be more suitable than RO membranes for this purpose, since they present better permeability, and hence less unwanted compounds rejection [Malmali et al., 2014]. Regarding the presence of salts, studies by Bouchoux et al. and Mohammad et al. have investigated the operation of polyamide flat-sheet NF membranes for sugar concentration and found that, when salt is present, the glucose rejection is lower. Bouranene et al. also studied the concentration of uncharged solutes along with the presence of salts in ceramic tubular NF membranes and observed a decreased solute rejection as well. Other studies for ceramic tubular NF membranes by Christopher and Caltran et al. revealed that ceramic NF membranes perform better than polymeric NF membranes when the thermal stability and flux values are concerned. Additionally, the same studies showed that the salt passage in the permeate is higher when the molecular weight cut-off (MWCO) is smaller. In addition, NF membranes can operate under higher fluxes and at lower pressures than the RO membranes, whereas the separation of sugars was proven to be better accompanied with limited membrane fouling [Murthy et al., 2005]. Furthermore, for polymeric membranes, the membrane charge and the pore size constitute major parameters that affect the separation process and NF membranes were proven to have more selectivity than RO membranes [Shirley et al., 2014]. Except for the advantages in separation, NF membranes are proven to be more dominant as far as the cost effectiveness is concerned, in comparison with conventional technologies for concentrating liquid streams. More specifically, NF membranes were proven to be more profitable for dehydration of feed solutions than other methods, such as the one of evaporation [Samee et al., 2016].

As already mentioned, apart from the NF technology, the process of concentrating sugars has also been tested with the MD technology. In the recent study of A Shirazi and Kargari, sweeping gas membrane distillation (SGMD) was used to concentrate glucose syrup, where high sugar retention was achieved. According to the study of Zhang et al., an almost complete glucose retention using the vacuum membrane distillation (VMD) process was also proven to be possible. The VMD unit with flat-sheet membranes is widely applied in fields of desalination or in cases of multi-component transport such as must and aroma compounds [Chiam and Sarbatly, 2013]. In order to desalinate solutions, VMD with flat-sheet membranes has proven to be a suitable technology, reaching a complete rejection at low flow rates, independently of the solution's temperature [Li and Sirkar, 2017]. To date, research on concentrating sugars with MD has mostly focused on the sugar rejection and it remains unclear whether the salts have an influence on the process of concentrating sugars. However, the separation of hydrolysis by-products from sugars, was studied by Zhang et al., showing that the simultaneous concentration of hydrolysates and removal of impurities is possible. More specifically, this study reported that the C5/C6 sugars can be concentrated by a factor of 3 with VMD coupled with prior adsorption, with a reported sugar loss of 2% in the permeate. More information on the different MD configurations are provided in Chapter 2, in Section 2.2.

1.3 PROBLEM DESCRIPTION

As presented in Section 1.2, it can be deduced that concentrating sugars has been widely studied over the years with different membrane technologies. However, it remains ambiguous which membrane technology is the most suitable to achieve high C5/C6 sugar concentration factors. Additionally, there is no comparative study for the application of membrane technologies that use different driving forces with the purpose of concentrating C5/C6 sugar streams, which also contain salt and sugar degradation products, while

maintaining the same experimental conditions and the same feed solution composition. The current research is aiming to investigate the extent of concentrating sugars with different membrane technologies and assess the performance of the most suitable one in terms of energy consumption.

While RO has been proven a suitable technology for concentrating sugar solutions, the presence of salt in the hydrolysate solution constitutes a limiting factor for the application of RO in the current study. An increasing sugar concentration will be accompanied by an increasing salt concentration. The latter will require high applied pressures in the system (> 40 bar threshold in applied pressure) as a result of the increasing osmotic pressure in the concentrate stream. Therefore, in this study, NF was chosen to be investigated as a concentration technology with the goal of 10 wt % concentration of C5/C6 sugars in the concentrate stream. The boundary conditions for the current research can be described as:

(i) lower than 10 % of total C5/C6 sugars in the permeate stream and
(ii) lower than 20% of salt rejection in the case of NF

Consequently, the main focus of the current study is to test and subsequently, assess the performance of (i) flat-sheet VMD and (ii) tubular ceramic and polymeric NF membrane units. Additional reasons behind the choice of these technologies for the treatment of the hydrolysate stream from Avantium were: (i) the previous unsuccessful attempts for concentrating the hydrolysate stream from Avantium with flat-sheet NF membranes due to significant fouling (see Figure B.1 in Appendix B), (ii) the need for high water recovery (iii) the higher permeate flux and minimum heat loss of the VMD in comparison with the other MD configurations [Li and Sirkar, 2017] and (iv) the available waste heat from the prior hydrolysis that can offer a significant advantage to the VMD operation.

1.3.1 Research objective

For the assessment of the NF and VMD technologies, the rejection of the C5/C6 sugars and salt and the permeation of water will be studied. The C5/C6 sugar rejection should be higher than 90 % in both membrane technologies to achieve the sugar concentration goal of 10 wt %. Therefore, the technology that will meet the rejection requirements will be further investigated for its ability to concentrate the C5/C6 sugars up to 10 wt %. Afterwards, the most suitable membrane technology for concentrating the C5/C6 sugars will be also assessed based on its energy consumption. Consequently, the ***research objective*** of the current MSc thesis research can be given as:

The identification and selection of the most suitable membrane technology with the purpose of concentrating C5/C6 sugars out of a stream containing salt and sugar degradation products.

1.3.2 Research questions

The research objective can be further formulated to a main research question and subsequently to sub-questions that need to be answered to achieve the research objective. Therefore, the main ***research question*** can be given as follows:

Among the different NF and MD membranes, which membrane is the most suitable for concentrating the C6/C5 sugars and what is the energy cost for this purpose?

And the following sub-questions that need to be addressed can be formulated as:

1. How does an increase in the driving force of the tubular NF influence the rejection of the C5/C6 sugars and the permeation of salt and water?

2. How does an increase in the driving force of the VMD influence the rejection of the C5/C6 sugars and salt and the permeation of water?
3. Among tubular ceramic and polymeric NF membranes, which membrane material facilitates the concentration of the C5/C6 sugars?
4. Is the 10 wt % concentration of the C5/C6 sugars feasible with the most suitable membrane technology?
5. What is the energy consumption of the most suitable technology for concentrating the C5/C6 sugars?

2 LITERATURE REVIEW

In this chapter, the characteristics of the NF and MD technologies and information regarding their application in sugar processing are provided. More specifically, in Section 2.1 the fundamentals of NF and specifics of tubular NF membranes are presented. Following the NF, Section 2.2 incorporates the most important characteristics and operational parameters of the MD technique. A more in-depth analysis for the VMD configuration, is also provided in this section. Lastly, Section 2.3, consists of a literature review on the energy consumption of different concentration technologies.

2.1 NANOFILTRATION

The pore size of the NF membranes falls in between UF and RO membranes [Bargeman et al., 2014]. Being a pressure-driven process, NF facilitates the filtration and retention of solutes with a size in the range of 100-1000 Da (with an approximated nominal membrane pore size of 1 nm), which could either be charged or not [Oatley et al., 2013]. Models regarding the separation of uncharged solutes in NF make use of the assumption that the membrane consists of straight cylindrical pores, in which the transport of the solute is corrected for hindered convection and diffusion as a result of the interaction between the solute and the membrane [Bowen and Welfoot, 2002]. The reduction in the solute's diffusivity in the pores of the membrane results in the rejection of the solute [Dechadilok and Deen, 2006]. The NF membranes are commercially diverse as far as the membrane charge and pore size are concerned and thus, the size and charge exclusion mechanisms differ among different membranes. These separation mechanisms can be described by introducing the terms of *steric hindrace* and *Donnan exclusion*, respectively [Murthy et al., 2005]. As a cross-flow filtration process, NF facilitates the passage of solvents and the retention of solutes. The pore blocking in the NF membranes can be described by introducing the term of *concentration polarisation*. The concentration polarisation phenomenon leads to an increase of solutes on the membrane surface which subsequently, leads to an increased resistance in permeation [Bellona et al., 2010]. For solutes that are uncharged like the C5/C6 sugars in the current study, the description of their transport in the membrane is mainly based on diffusive and convective flows [Bargeman et al., 2014].

The Donnan steric pore model (DSPM) has been widely used to describe the transport of solutes and solvent during the NF operation and in order to characterize commercial NF membranes in terms of effective (i) pore radius (r_p), (ii) membrane thickness/porosity ratio (Δ_x / A_k) and (iii) membrane charge density (X_d) [Mohammad, 2002]. The DSPM model takes into consideration the hindered convection and diffusion and originates from a modified and extended version of the Nernst-Plank model, which describes the transport of ions in NF membranes but with an exclusion of the steric effects and concentration polarisation phenomena [Mohammad, 2002]. The findings in the study of Bowen and Welfoot indicate that the rejection of uncharged solutes in the NF membranes is only dependant on the membrane's pore size. A mathematical formulation of the DSPM model can be seen in Appendix A, in Section A.1.

The NF technology constitutes a sustainable solution for sugar recovery, as it is characterised by a small footprint, ease of operation and no addition of chemicals [Guo et al., 2019]. Furthermore, NF is proven to be a promising technology for the separation

between two different kinds of sugar. With a sugar retention up to 90 %, NF can replace other cost inefficient technologies in bio-refineries, including the one of chromatographic separation [Roli et al., 2016]. However, the presence of salts in sugar solutions can cause a decrease in the sugar rejection as reported in the study of Luo and Wan, in which the NF application for the simultaneous retention of organic solutes, divalent ions and the permeation of multivalent ions was investigated. The diversity among commercial NF membranes encompasses challenges regarding (i) the appropriate membrane selection for the NF integration in sugar industries and (ii) the successful separation of sugars from salts [Mohammad et al., 2010]. It is important to also take into account the influence of the pH and the salt concentration on the membrane performance in terms of solute rejection, permeability and fouling behavior [Luo and Wan, 2013]. A study by Luo and Wan, investigated the rejection of organic solutes in the presence of inorganic salts on polymeric NF membranes. The findings from this research indicated that the presence of salts can result in a decreased solute size and an increased membrane pore size and effective thickness. Another study by Bargeman et al. on polymeric NF membranes validated that in the presence of high salt concentration, the sugar retention decreases as a result of the change in the ratio of sugar radius over the membrane pore radius.

Tubular Ceramic and Polymeric Nanofiltration

The tubular configuration of the NF membranes has the advantage of higher cross flow velocity in comparison with the spiral wound configuration with flat-sheet membranes and subsequently, it can have the advantage of less fouling phenomena [Kucera, 2019]. A study by Verissimo et al. introduced a new composite hollow fiber membrane, which was characterised by less demand in maintenance and higher packing density than spiral wound and tubular membranes. The hollow fiber module was tested for electrolyte and non-electrolyte solutions and the results regarding the non-electrolyte solutions demonstrated a lower sugar retention than the one observed in spiral wound and tubular membranes in other studies. However, an accurate comparison between these configurations is not possible due to the different operating conditions among different studies.

Most of the studies on the concentration of sugar solutes have focused on polymeric flat-sheet NF membranes proving the drawbacks of both material and configuration in fouling and cleaning. Therefore, the interest has been shifted to tubular modules and mostly to ceramic NF membranes. The ceramic NF membranes are designed to be more chemically, thermally and mechanically stable in comparison with the polymeric membranes [Árki et al., 2019]. Apart from the aforementioned characteristics, ceramic membranes are also characterised by high filtration fluxes, long life-time, bacterial resistance and easy cleaning. The disadvantage in their use is their high capital cost in comparison with polymeric membranes [Oliveira, 2018], [Sjölin et al., 2020].

The concentration of sugar beet sucrose molasses has been studied with ceramic NF membranes by Sjölin et al. and Oliveira, proving that ceramic NF membranes are suitable for the rejection of sugar from molasses. However, the concentration of hydrolysates from lignocellulosic biomass has only been studied with ceramic microfilters by Hasan et al. and it was primarily used to remove the turbidity of the solution so that it can be further treated with NF without the presence of severe fouling phenomena. The area of concentrating C5/C6 sugars with ceramic tubular NF membranes out of neutralized hydrolysate streams, has not been explored in depth.

2.2 MEMBRANE DISTILLATION

In comparison with the pressure-driven NF technology, MD is a thermally-driven microfiltration process, where a hydrophobic membrane allows only the passage of water vapour molecules on the permeate side of the module [Alkhudhiri et al., 2012]. The

driving force for the water transport is then created by the vapor pressure difference and hence, diffusion constitutes an important mechanism in the MD operation [Sundergopal et al., 2015]. With the potential of having very pure and high permeate flux, MD is used extensively in desalination processes and offers plenty of advantages, such as high rejection of non-volatile solutes with low operating temperature and pressure gradients [Li and Sirkar, 2017]. The MD technology can be found in four configuration types which are: (i) direct contact membrane distillation (DCMD), which is the simplest configuration; the hot feed solution is in direct contact with the hot side of the membrane surface, (ii) air gap membrane distillation (AGMD), where stagnant air is present between the membrane and condensation surface, (iii) SGMD, where inert gas sweeps the vapour of the permeate side to condensate outside of the membrane module and finally, (iv) VMD, where a pump creates a vacuum in the permeate side of the membrane and condensation happens outside of the module [Alkhudhiri et al., 2012].

Among the many advantages that the MD technology offers, there are some significant parameters that need to be taken into account for a successful MD application. As in every membrane process, organic and inorganic fouling can have negative consequences on the overall MD performance. The fouling originates from the accumulation of different components and can occur on the membrane's surface or in the pores of the membrane [Sinha Ray et al., 2020]. *Membrane wetting* is also a significant and particular characteristic of the MD membranes, as it can decrease the overall MD performance and deteriorate the quality of the permeate [Chang et al., 2020]. Most of the recent industrial effluents are complex and consist of various salts and organic components that can decrease the surface tension of the feed stream entering the MD and thus, enhance the possibilities of fouling and membrane wetting [Eykens et al., 2017]. During membrane wetting, the membrane loses its hydrophobic characteristics and the feed solution is passing through the membrane pores to the distillate side. Therefore, the separation begins to fail and the quality of the permeate is gradually decreasing, as the wetting, results in a repeated water bridging which finally leads to a fully wetted membrane. Fouling can be linked to the wetting phenomena in MD, as it does not allow the vapors to pass through the membrane but instead forces the vapors to condense inside the pores of the membrane. As a result, the membrane pores become full with the feed liquid which eventually passes to the permeate side [Sinha Ray et al., 2020].

The membrane wetting can be predicted and is linked with three important parameters, namely (i) contact angle (CA) (ii) surface tension (ST)/surface free energy (SFE) and (iii) liquid entry pressure (LEP). The liquid's CA on a hydrophobic surface should be larger than 90 ^{o}. The wetting will occur when the CA of the liquid will have values lower than 90 ^{o}, as it has been described by the Young's equation for smooth flat surfaces [Chang et al., 2020]. If the solution contains surface active agents (surfactants or generally, organic substances), the liquid surface tension of the solution will decrease and subsequently, the CA will drop as well [Franken et al., 1987]. The LEP [Pa] is described from the modified Young-Laplace equation (Equation 2.1) [García-Payo et al., 2000]:

$$LEP = -\frac{2\beta\gamma_l \cos\theta}{r_{\max}} > \Delta P_{\text{interface}} = P_{\text{liquid}} - P_{\text{vapor}} \tag{2.1}$$

where, P_{liquid} and P_{vapor} are the pressures [Pa] of the feed water and water vapor, respectively. The terms γ_l and θ are the surface tension of the feed liquid [N/m] and the CA [^{o}] of the liquid, respectively. The term β is the geometric factor that describes the geometry of the pores, and is assumed equal to 1 for cylindrical pores [Franken et al., 1987] and r_{max} is the maximum pore radius [m]. The pressure difference on the interface of the membrane should be lower than the LEP of the hydrophobic membrane to avoid the membrane wetting.

To calculate the SFE of a solid material, many methods such as the Zisman method, Fowkes model, Owens-Wendt-Rabel-Kaelbe (OWRK) and Lifshitz-van der Waals/Acid-base (LW-AB) methods have been proposed, each one with its own limitations. Among

them, the Fowkes model and Zisman approach should be used in case the membrane entails only known dispersive components. The OWRK method is taking into account both dispersive and non dispersive components based on two-liquid measurements and the LW-AB method is based on three-liquids measurements. OWRK and LW-AB methods are widely used for SFE calculations [Chang et al., 2020]. When the SFE of the MD membrane and the surface tension of the liquid are known, the membrane wetting can be predicted. In the study from Eykens et al., the wetting of polytetrafluorethene (PTFE), polyethylene (PE) and oleophobic polyethersulfone (PES) membranes, was investigated in the presence of surfactants in the feed solution. Based on the decreased surface tension along with higher surfactant concentrations, the wetting of the membrane was assessed based on the lower surface tension values in comparison with the surface energy of the membranes. According to the results of this study, the surface free energy of the PTFE and PES membranes was low enough and the wetting from the surfactant solution was avoided. The PE membrane was more prone to wetting after a certain surfactant concentration.

MD has been already studied as a technology for concentrating streams like fruit juice and sugar solutions. More specifically, in a study by Nene et al., sugar cane juice was processed with DCMD and it was found that MD can be a promising technology for concentrating sugars. More recent studies regarding the concentration of lignocellulosic hydrolysates or sucrose solutions through MD technology have shown that the sugar can be concentrated along with a very low percentage of sugar loss in the permeate [Zhang et al., 2012], [Chen et al., 2013], [Zhang et al., 2015] and in the case of sucrose, pure permeate water [Al-Asheh et al., 2006] can be retrieved. In the study of Zhang et al., the VMD technology has shown almost 100% glucose rejection from a hydrolysate feed water, with a maximum glucose concentration factor (CF) of 4. The aforementioned studies used the VMD configuration, because when compared with other MD configurations, VMD shows the minimum heat loss across the membrane and a higher vapour flux [Li and Sirkar, 2017] due to the higher partial pressure gradients that are allowed [Abu-Zeid et al., 2015].

However, the golden ratio between water vapor flux and energy consumption remains a challenge in the VMD operation [Li and Sirkar, 2017]. In the study of Zhang et al., the VMD unit coupled with solar energy has been proven to be a competitive treatment option for bio-refineries in comparison with conventional processes. A comparative study by Criscuoli et al., investigated the energy consumption between DCMD and VMD set-ups using pure water and it was found that the VMD performs better in terms of energy consumption, requiring 3 times less energy for the production of 1 kg of permeate. Another study by Duong et al., investigated the energy consumption of a single-pass pilot scale AGMD with spiral wound membranes for seawater desalination purposes, with integrated solar energy. The findings of the aforementioned study indicated lower energy consumption in case of AGMD when compared to an RO installation. Based on the advantages of the VMD configuration, the aim of the current study is to concentrate the C5/C6 sugars using this technique. A more in-depth description of the VMD configuration is thus given in the next section.

Vacuum Membrane Distillation

To achieve the research goals on concentrating sugars with VMD, the determination of the most important parameters that influence the VMD operation is necessary. The performance of the VMD is controlled by the vapor-liquid equilibrium [Zhang et al., 2015]. The mass transfer that occurs can be described by either the Knudsen or the viscous flow model (or a combination of both), depending on the ratio of membrane pore radius (r_p) over molecular mean free path (λ) [Abu-Zeid et al., 2015]. The heat transfer occurs based on the following steps: (i) heat transfer by convection from the hot feed solution on the hot side of the membrane through the thermal feed side boundary layer (ii) water evap-

oration and (iii) transfer of water vapour for condensation on the permeate membrane side. The heat transfer by convection is correlated with the *temperature polarisation* phenomenon in MD processes [Abu-Zeid et al., 2015]. During temperature polarisation, the temperature in the membrane interface is becoming lower than the temperature of the bulk, which leads to a decrease in the driving force during MD process and hence, results in a decrease of the mass transfer [Politano et al., 2019]. The MD process is then characterised by the resistance of a large boundary layer formation [Alkhudhiri et al., 2012] which can cause a reduction in the driving force of up to 80% [Abu-Zeid et al., 2015].

Another type of polarization in MD technique is the *concentration polarisation* that occurs when non-transporting components are accumulating on the membrane surface with bigger concentration than the one in the feed solution. Especially for multi-components processes, decreasing the concentration polarisation phenomenon can play a significant role when the rejection of a component and the permeation of another is targeted [Chiam and Sarbatly, 2013]. An additional important factor used to evaluate the MD performance is the thermal efficiency, which is proved to be higher when the temperature, the feed flow rate, and the membrane thickness are increased. Conversely, the thermal efficiency becomes lower when the solute concentration in the feed solution is increased [Alkhudhiri et al., 2012].

The flow conditions in the MD process are optimal when transitional or turbulent hydraulic conditions are applied, because there are less polarisation effects and more gas transport through the membrane [El-Bourawi et al., 2006]. The type of the flow is determined by the Reynolds number (Re). By increasing the Re, more unsteady flows can be achieved. For spacer-filled flow channels, the Reynolds number can be smaller than in the case of open channels. More specifically, in channels without the use of spacers, a turbulent flow requires Re values bigger than 2000 and in the case of applied spacers, a Re of 1000 is needed instead. Additionally, in spacer filled channels, Re values lower than 300 declare a steady flow, whereas when 350<Re<1000 the flow is characterised as fully unsteady [Mojab et al., 2014].

Other important factors that influence the efficiency of the VMD technology are the membrane characteristics and especially: (i) the LEP, which describes the maximum allowed applied pressure to prevent the penetration of liquid in the membrane (membrane wetting), (ii) the membrane thickness, where thicker membranes denote higher mass transfer resistance and hence lower permeate flux and heat loss, (iii) the membrane porosity and turtuosity (iv) the mean pore membrane size, which is used to determine the vapour flux and (v) the thermal conductivity, which when low, can lead to lower heat losses [Alkhudhiri et al., 2012].

2.3 ENERGY CONCERNS IN CONCENTRATION TECHNOLOGIES

As already mentioned in Section 1.2, concentrating sugars can be very energy intensive. Evaporators have been used in many industrial applications to concentrate liquid streams. The application of evaporators can be found in food processing, dairy, sugar and pharmaceutical industries as well. The efficiency of evaporators can be estimated from the term of *steam economy (SE)* which is determined as the ratio of the water evaporated and the steam consumed [Valentas et al., 1997]. Single-effect evaporators need approximately 1.1 kg of steam to evaporate 1 kg of water, which corresponds to a latent heat of vaporisation of 2700 KJ/kg of evaporated water [Schuck et al., 2015]. The SE of a single-effect evaporator lies in the range of 0.75-0.95 kg water/kg steam [Valentas et al., 1997]. In the case of multi-effect evaporators, the different effects/stages are connected and the liquid is passing from one stage to another, taking advantage of the vapor produced in every previous stage. This way, the latent heat of vaporisation can be computed as 2700/N KJ/kg water removed, where N are the stages of the multi-effect evaporator [Schuck et al., 2015]. Therefore, the SE of multiple-effect evaporators can be estimated as (0.75-0.95) x N (in kg water/kg steam), where N represents the number of the effects. Based on the latter relationship, the SE of an e.g. 3-effect evaporator will be in the range of 2.4-2.8 kg water/kg steam.

Improvements in the operation of the evaporators, such as thermal or mechanical vapor compression can lead to significant energy savings [Valentas et al., 1997]. However, the increase in the energy efficiency of evaporators with the addition of more effects is proportional to the capital costs. As far as the operational costs are concerned, the addition of more effects is inversely proportional with the running costs [Sarma and Barma, 2010]. In order to minimize the energy consumption in the operation of evaporators, a system integration with other processes has been proven to have a positive impact on the overall energy consumption [Sharan and Bandyopadhyay, 2016]. By knowing the power consumption, the distillate production and the steam required for the evaporation, the energy consumption in KWh/ kg of water evaporated can be computed. Table 2.1 provides the energy consumption of different evaporators in different fields of use.

Research on the energy consumption of MD units indicated an energy consumption of 90.2 KWh/m^3 of permeate production for an AGMD unit, used for desalination purposes [Duong et al., 2016]. Findings of an earlier research on the energy consumption of a DCMD versus a VMD unit, proved the efficiency of the VMD with an energy consumption of 1.1 KWh/kg of permeate instead of the consumption of 3.55 KWh/kg in the case of the DCMD unit Criscuoli et al. [2008]. In desalination plants, RO is the most dominant applied technology with an energy consumption in the range of 1-6 KWh/m^3 [Roy and Ragunath, 2018]. For distillation plants and thermal technologies, the energy consumption is defined as the energy consumed for the production of 1 m^3 of distilled water. A study by Madaeni and Zereshki found that pre-concentrating sugar solutions with a two-stage RO before using a multi-effect evaporator, can save up to 33% of consumed energy. In the MD technology, utilising waste heat can result in an energy consumption of 1.25 KWh/m^3 for an AGMD unit [Ullah et al., 2018]. The same study by Ullah et al., indicates that without waste heat available the energy consumption of a VMD unit can be larger than 9000 KWh/m^3. It can be seen that the energy consumption of the MD along with the utilisation of available waste heat, can be a viable option for concentrating liquid streams. Additionally, the combination of membrane and thermal technologies can lead to significant energy savings. However, the selection of proper concentration technologies and membrane characteristics, the development of sustainable and economic hybrid-processes and the optimisation of current treatment schemes as well, are crucial and challenging among different industries and applications [Roy and Ragunath, 2018].

Table 2.1: Different types of evaporators used in different fields and their energy consumption

Evaporator Type	Field of use	Energy Consumption (KWh/kg water evaporated)	References
Single evaporator	Sugar industry	0.59-0.62	Prado et al. [2015]
3-Effect evaporator	Sugar industry	0.49-0.51	Prado et al. [2015]
6-effect vacuum evaporator	Dairy industry	0.12	Schuck et al. [2015]
3-effect Evaporator	Bio-refinery	0.56	Sharan and Bandyopadhyay [2016]
3 effect evaporator + MVR	Dairy industry	0.06	Zhang et al. [2018]
5-effect Evaporator	Dairy industry	0.18	Zhang et al. [2018]

2.4 CHAPTER SUMMARY

While high sugar rejection values can be achieved with NF and MD technologies, the process of concentrating sugars can be limited by (i) the presence of salts and other solutes in the feed water, (ii) severe membrane fouling phenomena and by (iii) the need for high applied pressures. Regarding conventional concentration processes like the one of evaporation, thermal membrane technologies like MD can be a competitive option in terms of energy consumption. However, for the concentration of lignocellulosic hydrolysates, a proper selection of membrane properties and filtration technologies should be made, as the hydrolysates often contain sugar degradation products and monomeric sugars with small molecular weight (MW) that can affect the overall sugar concentration process.

3 MATERIALS AND METHODS

Following the literature review on the membrane technologies that will be used in the current study, in this chapter the materials & methods of the laboratory experiments are discussed. In Section 3.1, the characteristics and composition of the feed water are provided. For both NF and MD, the experimental procedures, specific membrane characteristics and laboratory set-ups are given in Section 3.2, 3.3 & 3.4 respectively. The operational parameters for both membrane filtration technologies are presented in Section 3.5. As far as the NF is concerned, the methodology for the membrane pore radius calculation is described in Section 3.6, whereas in the following Section 3.7, the steps & analytical methods for the calculation of the performance parameters in both technologies are offered. Section 3.8 provides a more in-depth analysis on the MD membrane characteristics. More specifically, this section includes the methodology for the surface tension and contact angle measurements that were conducted for the MD membrane. Finally, Section 3.9 offers a detailed description for the energy calculations of the VMD set-up.

3.1 FEED SOLUTION

The feed solution was provided from Avantium with a concentration of 1 wt % C5/C6 sugars and 1 m% of HCL, as a result of the two-step hydrolysis of the lignocellulosic biomass. Among the C5/C6 sugars in the feed water, there was also a concentration of 0.5 wt % of hydrolysis by-products. A stream neutralization with NaOH secured the safety of the operations during the laboratory procedures and removed the stream's acidity for Avantium's downstream processes. With the addition of 1.08 wt % NaOH, the amount of NaCl was calculated to be 1.6 wt %. Therefore, the final feed solution to be treated, entailed C5/C6 sugars and salt, with a pH in the range of 7-8, instead of the initial pH range of 0.3-0.5. The composition of the feed solution in sugars and by-products can be seen in Table 3.1. The exact C5/C6 sugars and by-products concentration was derived from HPLC and IC analysis conducted in Avantium. From now on, the term *C5/C6 sugars* will be used to describe the mixture of pentoses and hexoses monosaccharides in the feed solution and the term *hydrolysate solution* will be used to denominate the (neutralized) feed water provided by Avantium.

The feed water provided by Avantium can be seen in Figure 3.1, prior and after the neutralization with NaOH. The color of the water can be partially explained by the presence of sugar degradation products. Apart from the sugar by-products presented in Table 3.1, the color of the feed water indicates the existence of additional substances. With an increase in pH (≥ 5), polymeric by-products can be produced from the HMF [Steinbach et al., 2017]. These by-products can refer to soluble humins (MW of 500-1000 g/mol) which could be responsible for the dark color of the liquid [Van Zandvoort, 2015]. Additionally, the feed water might also contain acid-soluble lignin [Wang et al., 2018] and pseudo-lignin compounds as a result of the acid pre-treatment of the lignocellulosic biomass [Meng and Ragauskas, 2017]. The MW of the lignin molecules can vary between 0.1-400 kDa [Humpert et al., 2016] and because they consist of phenolic compounds, the potential presence of these molecules could justify the dark brown color of the feed solution as well [Oriez et al., 2020]. It is important to also mention that apart from the monomeric sugars, the sugar by-products and the NaCl, the hydrolysate solution is also expected to contain

metal ions [Tokareva et al., 2007] with most abundant those of calcium, potassium and magnesium followed by iron, manganese and sodium ions [Su, 2012].

Table 3.1: C5/C6 sugars and by-products composition in the hydrolysate solution in wt %

(a) C5/C6 sugars composition [wt%]

Monomeric sugars	Concentration
Arabinose	0.06
Rhamnose	0.01
Galactose	0.17
Glucose	0.32
Xylose	0.10
Mannose	0.31
Total	0.97

(b) By-products composition [wt%]

By-products	Concentration
Hydroxymethylfurfural	0.01
Furfural	0.07
Formic acid	0.13
Levulinic acid	0.26
Total	0.46

Fig. 3.1: Hydrolysate solution before (left) and after (right) the neutralization with NaOH

3.2 EXPERIMENTAL PROCEDURES

To assess the concentration of sugars with tubular NF and VMD, the experimental procedures were divided in two phases (Phases I and II). During Phase I, the different ceramic and polymeric NF membranes were assessed based on their performance in C5/C6 sugar rejection. Due to the complexity in the composition of the hydrolysate solution, the membranes were first tested with synthetic solutions and their performance was assessed based on the rejection of the sugars (glucose and xylose) in the synthetic solution and the permeation of NaCl and water. More specifically, the experiments of Phase I were conducted using the following solutions and concentrations:

1. Demineralized water (permeability test)
2. Synthetic NaCl solution (1.5 wt %)
3. Synthetic glucose (1.4 wt %) and NaCl (1.5 wt %) solution
4. Synthetic xylose (1.4 wt %) and NaCl (1.5 wt %) solution
5. Neutralized hydrolysate solution

For the synthetic solution experiments of Phase I, NaCl 99.5 % and D(+)-Xylose, 99+% were purchased from ACROS Organics^{TM}, whereas D + (-) - Glucose, anhydrous, GPR RECTAPUR® and L (+) - Rhamnose monohydrate, PanReac AppliChem were purchased from VWR CHEMICALS. The aforementioned 5 solutions were used to assess the performance of two ceramic NF membranes, with MWCO of 450 and 200 Da and two polymeric NF membranes (AFC30 and AFC40), for which there were no MWCO specifications provided by the manufacturer. For the VMD unit, one PTFE hydrophobic membrane with a pore size of 0.2 μm was used. A more detailed description of the NF and MD membranes used is given in the following Sections 3.3.1 & 3.3.2. In the case of the VMD, a synthetic mixture of C5/C6 sugars was used as the feed solution, rather than separate C5/C6 synthetic solutions, as the separation in VMD process is based on the hydrophobic attribute of the membrane. Therefore, only the permeation of water vapor and volatile substances is expected. The concentrations of xylose, glucose and NaCl in the synthetic solutions were determined based on the concentrations expected in the hydrolysate solution. *The goal of Phase I was to achieve >90% rejection of the C5/C6 sugars with a NaCl rejection lower than 20 % in the case of NF membranes.*

The goal of Phase II of the experimental procedures was to investigate if the C5/C6 sugars can be concentrated up to 10 wt % with the membrane/technology that had the best performance during Phase I. *Therefore, the concentration goal of Phase II was to achieve a 10 wt % concentration of C5/C6 sugars and hence, approach 90 % of water recovery in the initial feed solution.*

3.3 MEMBRANE CHARACTERISTICS

3.3.1 Nanofiltration membranes

The ceramic NF membranes were supplied from INOPOR and their characteristics can be seen in Table 3.3. The sealing of the membranes is made with glass, while the membrane with the MWCO of 200 Da is the ceramic membrane with the smallest MWCO that INOPOR has recently manufactured. The details of the polymeric membranes provided by PCI are presented in Table 3.4. The active surface area of the membranes was 118 cm^2 for the polymeric membranes and 110 cm^2 for the ceramic membranes.

Table 3.3: Characteristics of the ceramic tubular NF membranes used for experiments

Membrane ID	Material	Pore Size	MWCO	Porosity
A3T09G	TiO_2	0.9 nm	450 Da	30%-40%
A3LC1G	TiO_2	-	200 Da	30%-40%

Table 3.4: Characteristics of the polyamide tubular NF membranes used for experiments

Membrane ID	Material	pH range	Operating pressure	Operating temperature	Retention Character	Hydrophilicity
AFC40	Polyamide film	1.5-9.5	60 bar	60 ^oC	60% $CaCl_2$	high
AFC30	Polyamide film	1.5-9.5	60 bar	60 ^oC	75% $CaCl_2$	high

3.3.2 Membrane distillation membranes

The flat-sheet membrane used in the VMD set-up was provided by Sterlitech (Kent, Washington USA) with characteristics as described in Table 3.5. The active surface area of the

MD membrane was 34 cm^2. The 47 Mil Diamond feed and 31 Mil Diamond permeate spacers were also provided by Sterlitech.

Table 3.5: Characteristics of the PTFE flat-sheet MD membrane used for experiments

Membrane ID	Material	Pore size	Support material	Water entry pressure	Application Temperature	Thickness	pH
1121838	PTFE	0.2μm	laminated PP neting	>2.5 bar	82 ^oC	76-152 μm	1-14

3.4 EXPERIMENTAL SET-UP

3.4.1 Nanofiltration

The experimental set-up for the ceramic and polyamide NF membranes can be seen in the scheme of Figure 3.2. The set-up is designed for being able to accept both membrane housings. According to this scheme, a feed pump can take the solution under high pressure (up to 40 bars) out of the feed tank (with a minimum and maximum volume of 4.5-6 L, respectively), with a cross-flow range of 4-10 L/min. The permeate stream that is produced can be collected in a permeate tank where the concentrate stream recirculates to the feed tank. All along the process, flow and pressure indicators were used to provide all necessary measurements. A temperature indicator in the feed tank ensured the stable temperature throughout the process. The actual laboratory NF set-up with different membrane housings can be seen in Figure 3.3.

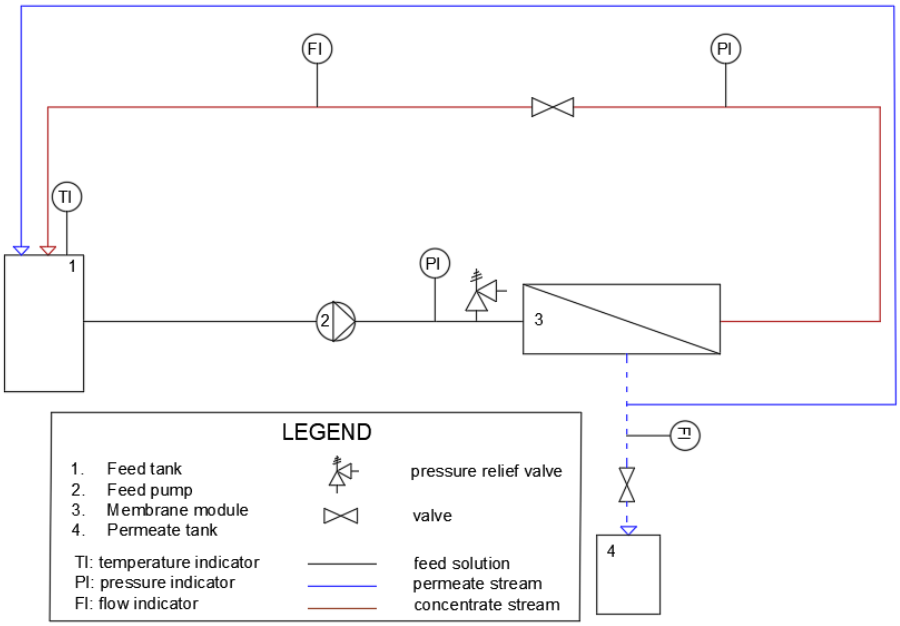

Fig. 3.2: Schematic drawing of the Nanofiltration set-up for both tubular and ceramic membranes

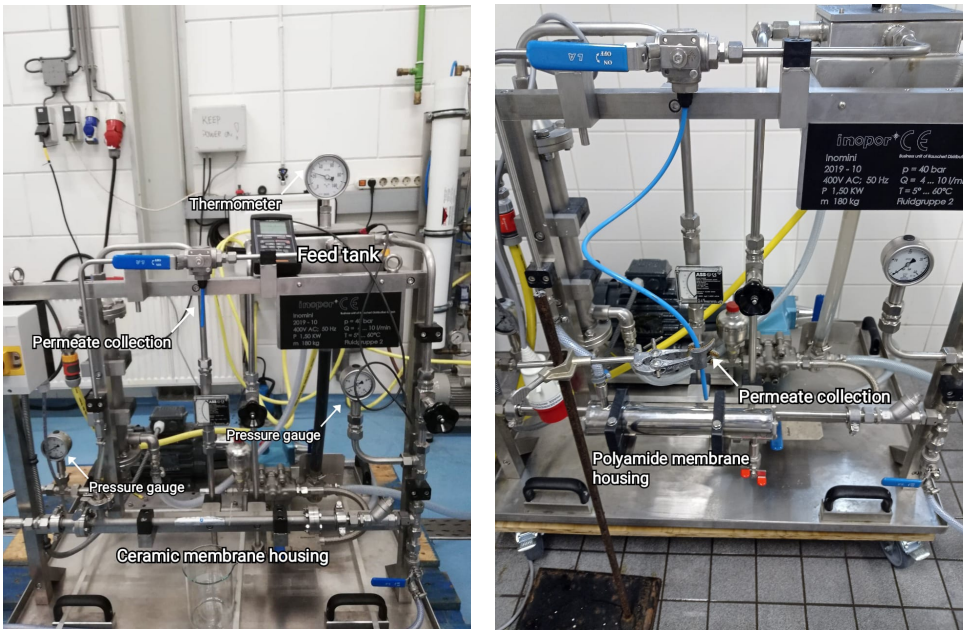

(a) Nanofiltration set-up with ceramic membrane housing

(b) Nanofiltration set-up with polyamide membrane housing

Fig. 3.3: Nanofiltration set-up with alternating polyamide and ceramic membrane housing

3.4.2 Vacuum Membrane Distillation

In the case of VMD, the experimental set-up can be seen in Figure 3.4. The solution flow in the system is ensured by turning on the feed pump. When the system is filled with water, the starting of the vacuum pump initiates the operation of the VMD. Sensors in the feed tank were constantly measuring the pH, electrical conductivity (EC) and the temperature throughout the experiments, while data logging of the EC and mass decrease also occurred. The feed tank was placed on a magnetic stirrer/heating plate; for efficient solution mixing and heating and on a digital balance; which was constantly measuring the weight of the solution. The concentrate stream was recirculating in the feed tank, whereas the permeate stream was connected to the vacuum pump. Pressure gauges were installed in the feed and permeate side of the set-up. Between the membrane cell and the vacuum pump, two gas scrub bottles immersed in an ice bath were included for condensation of the produced water vapor. A schematic drawing of the experimental VMD set-up is presented in Figure 3.4. The actual VMD set-up that was used in the laboratory experiments can be seen in Figure 3.5 .

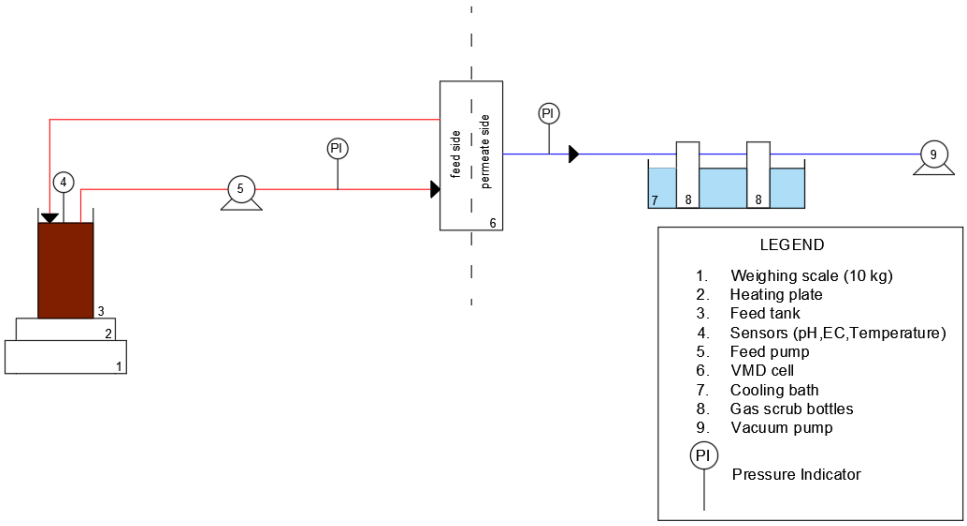

Fig. 3.4: Schematic drawing of the vacuum membrane distillation set-up

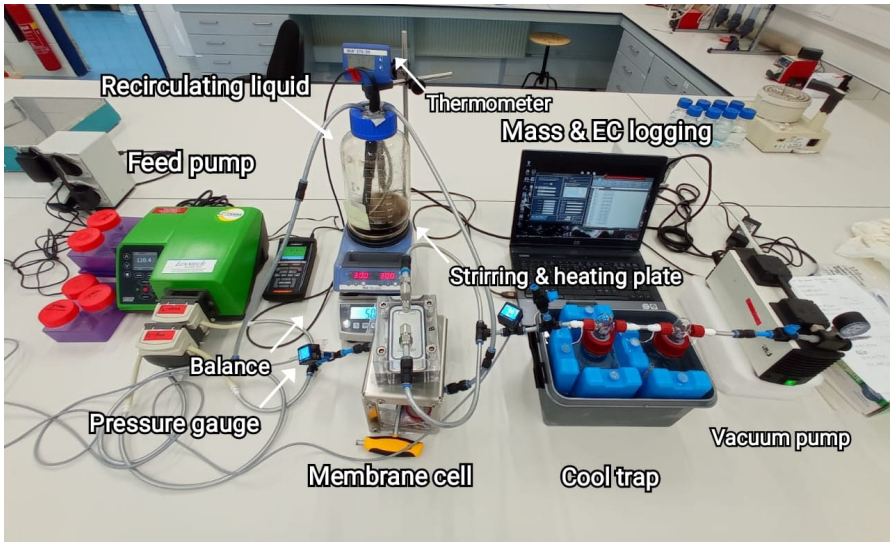

Fig. 3.5: Laboratory set-up of the vacuum membrane distillation unit

3.5 OPERATIONAL CONDITIONS

3.5.1 Nanofiltration

The desired flow for the NF membranes was set as turbulent to reduce the polarisation effect due to higher solute concentration as proposed by Magalhaes et al.. The maximum cross-flow rate of 10 L/min was held constant for both types of NF membranes. For Phase I of experimental procedures, the rejection values for all membranes and solutions tested were found for 10, 30 and 50 LMH of permeate flux, by altering the pressure in the set-up. The sampling was done after stabilization of the system for 1 hour in between the different fluxes. The temperature throughout the experiments was kept constant at 26 $\pm 1^{o}$ Celsius. The operation parameters for the NF experiments can be seen in Table 3.6, where the terms $NF-C_{1,2}$ and $NF-P_{1,2}$ refer to the two different ceramic and polymeric membranes, respectively. The formulas and hydraulic calculations for the tubular NF can be seen in section A.2.1 of the Appendix A.

Table 3.6: Operational parameters for the NF experiments during the Phase I of experimental procedures

Nanofiltration Membranes	Permeate Flux ($L/m^2/h$)	Temperature (^oC)	Cross-flow rate (L/min)	Cross-flow velocity (m/s)	Reynolds number (-)
NF-C1 **NF-C2**	10	26 ±1	10	4.33	18486
	30	26±1	10	4.33	18486
	50	26±1	10	4.33	18486
NF-P1 **NF-P2**	10	26±1	10	1.36	10352
	30	26±1	10	1.36	10352
	50	26±1	10	1.36	10352

3.5.2 Vacuum Membrane Distillation

The flow in VMD experiments was also set to unsteady/turbulent conditions based on a Re number of 400 to reduce the concentration polarisation phenomena and the possibility of membrane wetting. The hydrolysate solution is expected to have a temperature of 50^{o}C after the two-step hydrolysis. Therefore, during Phase I, the rejection of the C5/C6 sugar and NaCl mixture was assessed by applying a feed temperature in the range of 40-50^{o}C, with a temperature step of 5^{o}C. The operational conditions for the VMD are presented in Table 3.7. The formulas and hydraulic calculations for the MD unit and spacer filled channels can be seen in section A.2.2 of the Appendix A.

Table 3.7: Operational parameters for the VMD experiments during the Phase I of experimental procedures

MD Membrane	Applied Temperature (^oC)	Cross-flow rate (L/min)	Cross-flow velocity (m/s)	Reynolds number (-)
MD_1	40	0.56	0.13	400
	45	0.52	0.12	400
	50	0.48	0.11	400

3.6 PORE RADIUS EXPERIMENTS

In addition to the experiments of Phase I, pore radius determination experiments for the NF membranes were conducted. The methodology that was followed for these experiments was based on the study from Micari et al. [2020], in which pore radius experiments were conducted to characterize commercial NF membranes. The choice of the uncharged solutes for these experiments was made based on the difference in the MW of the sugars in the real hydrolysate solution. More specifically, glucose, rhamnose and xylose with characteristics given in Table 3.8, were chosen for this purpose. The reason behind the choice of the specific monomeric sugar molecules was to study the difference with regards to the rejection of single sugars that are already in the composition of the feed water provided by Avantium. Therefore, three different solutions containing separately the three different monomeric sugar molecules were investigated with the NF membranes. The concentration of each of the monomeric sugars was 200 mg/L in order to minimise the concentration polarisation phenomena in addition with the high cross-flow velocity that was applied to system [Micari et al., 2020].

The hydraulic parameters for the pore radius experiments were held the same as seen in Section 3.5.1. However, the rejection of sugar solutes was investigated for 35, 50, 105 and 170 LMH of permeate flux. There is a strong correlation between the rejection of the uncharged solutes and the applied pressure. With a higher applied pressure, the solute rejection is increasing as well, as there is higher water permeability and thus, more uncharged solutes stay in the retentate stream [Ghazali and Razak, 2021]. However, after a certain point the increase of the applied pressure does not contribute to the solute rejection anymore and there is a plateau in the rejection values. This phenomenon can be explained by the effect of concentration polarisation in the membrane wall that counterbalances the high convective fluxes and therefore, the transport of solutes in the permeate stream. The rejection that corresponds to the maximum and, subsequently, stable rejection of solutes is called *limiting rejection* (R_{lim}) [Labban et al., 2017]. For this reason, higher permeate fluxes were chosen in order to ensure that the R_{lim} was reached. The hindered transport is described through the hindrance factors $K_{i,c}$ and $K_{i,d}$, for convection and diffusion respectively. The following equations have been used to calculate the theoretical rejection of the three monomeric sugar solutes. The diffusion coefficient of a solute inside the membrane pores ($D_{i,pore}$), is given in Equation 3.1. The $D_{i,pore}$ is dependant on the diffusion coefficient of the solute in the bulk ($D_{i,\infty}$) and on the hindered diffusive mass transfer coefficient ($K_{i,d}$). The solute's theoretical rejection is given in Equation 3.2.

$$D_{i,pore} = K_{i,d} \times D_{i,\infty} \tag{3.1}$$

$$R_i = 1 - \frac{C_{i,p}}{C_{i,f}} = 1 - \frac{K_{i,c} \times \Phi_i}{1 - (1 - K_{i,c} \times \Phi_i) \times \exp(-Pe_i)} \tag{3.2}$$

where $K_{i,c}$ and $K_{i,d}$ are the hindered convective and diffusive mass transfer coefficients [-], which are given in Equations 3.4 & 3.5, respectively ; the term Pe_i is the Peclet number given in Equation 3.3.

$$Pe_i = \frac{k_{i,c} \times J_v \times \delta_m}{D_{i,p}} = \frac{k_{i,c} \times r_p^2}{8 \times \eta \times D_{i,p}} \times \Delta P \tag{3.3}$$

$$K_{i,c} = \frac{1 + 3.867 \times \lambda_i - 1.907 \times \lambda_i^2 - 0.834 \times \lambda_i^3}{1 + 1.867 \times \lambda_i - 0.741 \times \lambda_i^2} \tag{3.4}$$

$$K_{i,d} = \frac{\begin{array}{c} 1 + 9/8 \times \lambda_i \times \ln(\lambda_i) - 1.56034 \times \lambda_i + 0.528155 \times \lambda_i^2 + 1.91521 \times \lambda_i^3 \\ -2.81903 \times \lambda_i^4 + 0.270788 \times \lambda_i^5 + 1.10115 \times \lambda_i^6 - 0.435933 \times \lambda_i^7 \end{array}}{\Phi_i} \tag{3.5}$$

where λ is the ratio of solute radius to pore radius. The steric coefficient is given in Equation 3.7, and the limiting solute rejection in Equation 3.8.

$$P_{e\,i}{}' = \frac{K_{i,c} \times J_v \times \delta_m}{D_{i,p}} = \frac{K_{i,c} \times r_p^2}{8\eta \times D_{i,p}} \times \Delta P \tag{3.6}$$

$$\Phi_i = (1 - \lambda_i)^2 \tag{3.7}$$

$$R_{lim} = 1 - K_{i,c} \times \Phi_i \tag{3.8}$$

The theoretical rejection curve of each monomeric sugar molecule was fitted to the experimental rejection by minimising the sum of squared errors. The statistical error function is given in Equation 3.9 as the sum of squared errors (SSE) between the experimental and calculated solute rejection. The pore radius of each membrane was derived from the average pore radius of the three solutes.

$$SSE = \sum_{i} (R_{i,exp} - R_{i,calc})^2 \tag{3.9}$$

Table 3.8: Stokes radii, diffusivities, and molecular weights of glucose, xylose and rhamnose

Solute	Molecular Weight* (g/mol)	Diffusivity D_∞ ($10^{-9} m^2/s$)	Stokes radii r_s (nm)	Source for diffusivity and Stokes radii
Glucose	180.16	0.690	0.365	Labban et al. [2017]
Xylose	150.13	0.769	0.300	Labban et al. [2017]
Rhamnose	164.16	0.700	0.490	Clark and Konermann [2004] Jenkins and Bell [1987]

* The MW values for the sugar solutes are taken from [Lide, 2004]

3.7 ANALYSIS AND CALCULATION OF PARAMETERS

3.7.1 Analytical methods and calculation parameters

Concentrate and permeate samples were collected for every experimental run in both NF and VMD set-ups. The pH and temperature were measured with sensors and the presence of NaCl was determined with EC probes, based on a calibration curve. The presence of sugars in every sample was primarily determined with a chemical oxygen demand (COD) analysis in Lenntech, using the MACHEREY-NAGEL Spectrophotometer, NANOCOLOR UV/VIS II. In the case of the hydrolysate solution the samples were sent and analysed in Avantium, with Ion chromatography (IC) and High pressure liquid chromatography (HPLC) analysis for the determination of the presence of monomeric sugars and by-products, respectively. The hydrolysate samples were diluted and filtered with a 0.45 μm PTFE filter prior to the analysis in Avantium. The concentration of formic and levulinic acid was quantified with a refractive index (RI) detector, whereas the HFM and furfural with a diode-array detection (DAD) detector at 230 nm. The column used in HPLC method is the Aminex HPX-87H (300 x 7.8 mm; dp 9μm) column.

The rejection of sugars and salt can be calculated based on Equation 3.10 and the CF based on Equation 3.11 [Amjad, 1993].

$$\%R_i = (1 - \frac{C_p}{C_f}) \times 100 \tag{3.10}$$

where C_p and C_f are the concentration of the solute in the permeate and feed solution, respectively.

$$CF = \frac{1}{1 - \%R_w} \tag{3.11}$$

As far as the operation of NF membranes is concerned, the flux (J) and the osmotic pressure ($\Delta\pi$) are important parameters to consider, as they affect the overall membrane performance. The water flux can be computed according to Equation 3.12 [Amjad, 1993]:

$$J = \frac{V}{At} \tag{3.12}$$

where V is the permeate volume that is collected [L] per unit of membrane area (A) [m^2] and per unit time (t) [h]. The osmotic pressure is given in Equation 3.13:

$$\Delta\pi = \upsilon_i \times c_i \times R \times T \tag{3.13}$$

where, c_i is the concentration of total dissolved solids (TDS) [mol/L], υ_i is the number of ions from the solute dissociation, R is the universal gas constant [8.314 J/K/mol] and T is the absolute temperature [K].

Additionally, for the NF operation Equation 3.11, can not be used because it assumes a solute rejection of 100 %. Therefore, the CF for the NF operation can be calculated based on Equation 3.14 [Bi et al., 2014].

$$CF = \frac{C_c}{C_f} = \frac{1 - R_w \times (1 - r_o)}{1 - R_w} \tag{3.14}$$

where R_w is the water recovery and r_o the observed solute rejection.

3.7.2 Mass Transfer coefficient calculations

The mass transfer coefficient (MTC) for both NF and MD membranes tested was calculated based on the flux of the system and the pressure difference between the feed and permeate side. Equation 3.15 is the mathematical formulation of the MTC, for both systems, where J is the flux of the system and ΔP [Pa] the pressure difference between feed and permeate streams ($P_f - P_p$). In case of NF set-up, the flux was measured with a volumetric cylinder (2ml) and a timer, after the system's stabilization.

$$MTC = \frac{J}{\Delta P} = \frac{J}{P_f - P_p} \tag{3.15}$$

As far as the VMD is concerned, the MTC is linked to the global MTC, which takes into account the temperature polarization [Mengual et al., 2004] and based on the Equation 3.15, anticipates that the flux (J) is an exponential function of the temperature [Zhang et al., 2010]. The flux in VMD was determined based on the mass logging and scale measurements. The permeate vapor pressure was measured equal to 1500 Pa for a given applied vacuum in the permeate side, whereas the feed vapor pressure was determined using PHREEQC for a solution containing sugars and salt [Parkhurst and Appelo, 2013]. Because of the small concentration of by-products (in comparison with the water content and the sugar and salt components) and their partial transport in the permeate side during the VMD operation, their influence on the MTC calculations and PHREEQC modelling was considered as negligible.

In the PHREEQC model output, the saturation index (SI) of each solution component was computed. Based on the SI, the partial pressure of each component was calculated in units of atm. Based on Equation 3.16 the value of the partial pressure ($P_{i,f}$) depends on the fugacity coefficient (ϕ), which corrects for gas non-ideality, and the SI of the targeted component. For the current study, the component that was targeted in the VMD operation and MTC calculations was the water vapor.

$$P_{i,f} = \frac{10^{SI}}{\phi} \tag{3.16}$$

For low pressures (<10 atm), the fugacity coefficient can be considered equal to 1 [Parkhurst and Appelo, 2013]. Considering that 1 atm equals 101325 Pa, the $P_{i,f}$ was calculated by multiplying the numinator of Equation 3.16 with 101325.

3.8 CONTACT ANGLE AND SURFACE TENSION MEASUREMENTS

To investigate the effect of organic by-products and sugars on the hydrophobicity of the MD membrane, surface tension and contact angle measurements were done for the PTFE membrane. Demineralized water, NaCl solution, synthetic mixture of NaCl and sugars, and the hydrolysate solution were tested for their surface tension and contact angles on the hydrophobic membrane. For the contact angle measurements, four different parts of the active surface membrane area were selected to investigate the hydrophobicity along the membrane surface area based on different solutions.

Contact angle measurements

The contact angle measurements were conducted in the Materials Science and Engineering laboratory (3ME) of TU Delft. A theta Lite optical tensiometer was used for the contact angle measurements. The instrument was connected to the Full One-Attention Software which provided the values for contact angles with automatic baseline detection. The method that was followed for this purpose was the sessile drop method, in which a liquid droplet of around 3μL was manually formed with the help of a syringe and then was released and recorded as it was reaching the surface of the membrane. The membrane that was used was a pristine PTFE MD membrane that was soaked in demineralized water prior to the contact angle measurements. The different liquids and the membrane were under room temperature throughout the measurements. The contact angle measurements were conducted for different parts of the active surface membrane area and the average value was used in the SFE calculations of the MD membrane.

Surface tension measurements

The hydrolysate solution was also investigated for its surface tension based on different water recovery values. The surface tension measurements were conducted in the laboratory of Geoscience & Engineering of TU Delft, with EZ-Piplus tensiometer (Kibron Inc.), where a Du Noüy ring is incorporated with a microsize probe of 0.51 mm diameter. The samples were measured at room temperature and the ring was rinsed with demineralized water and dried after each measurement.

Membrane's surface free energy calculation with the OWRK model

As described in Section 2.2, there are several models for the calculation of the surface tension of a solid material, using contact angle and surface tension measurements. The SFE has been an important indicator of the wettability of a solid material. In the current study, the OWRK model will be used to calculate the SFE of the PTFE MD membrane. According to the modified Fowkes model, the liquid surface tension and the surface tension of the solid are analysed based on their polar and nonpolar components. The mathematical formulation of the OWRK model combines the Young and Young-Dupree models and is described as follows [Kozbial et al., 2014]:

$$\frac{\gamma_l \times (\cos\theta + 1)}{2} = (\gamma_l^d)^{1/2} \times (\gamma_s^d)^{1/2} + (\gamma_l^p)^{1/2} \times (\gamma_s^p)^{1/2} \tag{3.17}$$

where γ_l is the surface tension of the liquid [mN/m] and θ is the contact angle that forms the liquid droplet on the solid surface [^{o}]. The terms γ_l^d & γ_s^d are the liquid and solid dispersive components, respectively. The terms γ_l^p & γ_s^p are the liquid and solid polar components, respectively. According to the model, the surface tension of a solid surface can be eventually derived from Equation 3.18 :

$$\gamma_s = \gamma_s^d + \gamma_s^p \tag{3.18}$$

To calculate the SFE of the current PTFE, the contact angles of two liquids with known surface tension properties were measured. First, the contact angle of demineralized water

was measured, which has known dispersive and polar components. The other liquid that was used for this purpose was diiodomethane, which is a non-polar liquid ($\gamma_l^p = 0$), whose surface tension is also known. The purpose of testing these two liquids was to first find the dispersive component of the solid's surface tension using the properties of diiodomethane and then be able to calculate the polar component as well, with the known surface tension components of demineralised water. The properties of these two liquids can be seen in Table 3.9 [Shaker and Salahinejad, 2018].

Table 3.9: Values for surface tension of the dispersive & polar components of demineralized water and diiodomethane

Liquid	γ_l	γ_l^p	γ_l^d	Units
Water	72.8	46.4	26.4	mN/m
Diiodomethane	50.8	0	50.8	mN/m

3.9 ENERGY CALCULATIONS FOR THE VMD UNIT

The energy calculations for the VMD set-up, were made according to the study of Xie et al. based on which, the energy that is required for the VMD operation, can be calculated based on Equation 3.19.

$$E_{total} = E_1 + E_2 + E_3 + E_4 \tag{3.19}$$

where, (i) E_1 is the thermal energy required for the heating of the feed water
(ii) E_2 is electrical energy required for the feed re-circulation
(iii) E_3 is the electrical energy required for the operation of the vacuum pump and
(iv) E_4 is the thermal energy required for the permeate cooling and condensation.

Breaking down each term of Equation 3.19, Equations 3.20,3.21 and 3.22 can be defined in order describe the E_2, E_4 and E_3 terms, respectively. Due to the prior hydrolysis of feed water in high temperature gradients, the E_1 term can be eradicated, as it is assumed that there is waste heat available for the VMD process. Therefore, the heating of the feed water is not applicable in this case and thus, the energy requirement of this step will not be considered. The temperature of the feed water that will be used for the energy calculations is assumed to remain stable at 50^oC throughout the VMD operation and is ensured with the constant operation of a heating plate. The choice of the temperature value was made based on the sugar concentration experiment with the VMD set-up and according to the background information of the current project. Looking back to Equation 3.19, the following equations for the energy requirements of the feed stream recirculation and permeate cooling can be now defined [Xie et al., 2016].

$$E_2 = \frac{\Delta P_f \times V_f}{\epsilon_{pl}} \tag{3.20}$$

where, ΔP_f is the pressure drop in the feed side due to friction. The pressure drop was measured equal to 0.5 bar (relative to the atmospheric pressure), with the installation of a pressure gauge in the set-up. V_f is the volumetric flow rate of the feed, and ϵ_{pl} is the efficiency of the feed pump. The energy required for the operation of the cooler is defined in Equation 3.21.

$$E_4 = m_p \times \lambda + m_p \int_{T_{pi}}^{T_{pc}} C_{pg} \times dT + m_p \int_{T_{pc}}^{T_{po}} C_{pl} \times dT \tag{3.21}$$

where, λ is the latent heat of vaporisation, m_p is the mass flow rate of the permeate and T_{pi}, T_{pc} and T_{po} is the temperature value at the inlet, condensation and outlet of the permeate respectively. Additionally, C_{pg} and C_{pl} are referring to the heat capacity of

the water vapor and liquid, respectively. The first term of equation 3.21 concerns the latent heat of vaporisation, while the second term deals with the thermal energy that is required for the water vapor to reach the condensation temperature. The third part of Equation 3.21, concerns the thermal energy that is required for the condensate to reach a temperature lower than that of the condensation. This term can be eliminated in this case, as the temperature that was held in the cooler is assumed as stable and equal to the temperature required for condensation. Therefore, the subcooling energy will not be considered in this case. Additionally, industrial chillers operate with a certain coefficient of performance (COP). A high value for the COP can be translated to lower energy requirements for the VMD operation. In this study, the COP of the cooler is assumed to be 4, considering that it is a reasonable value for industrial cooling systems, as presented in the study of da Silva Pereira et al.. Because the energy calculations will be conducted based on the operation of a lab-scale VMD unit, *two different scenarios* will be considered for the operation of the cooler: One with 1:1 ratio of efficiency (*lab-scale scenario*) and one with an efficiency ratio of 1:4 (*industrial scenario*) to approach the energy requirements of industrial coolers.

Furthermore, the electrical energy required for the operation of the vacuum pump will be calculated based on the study from Huttunen et al.. Throughout the VMD concentration experiment a diaphragm, positive displacement pump was utilized. Based on the aforementioned type of the vacuum pump, an isentropic model for the operation of the vacuum pump is assumed [Allen, 2009]. Therefore, for an isentropic compression and assuming a complete system insulation, the following formula for the energy consumption of the current dry vacuum pump is derived as:

$$E3 = \frac{P_S}{\eta_S} \tag{3.22}$$

where, P_S is the isentropic power and η_S is the isentropic efficiency. The isentropic power of the pump is given in Equation 3.23.

$$P_S = \frac{k}{k-1} \times q_{V,in} \times P_{in}[(\frac{P_{out}}{P_{in}})^{\frac{k-1}{k}} - 1] \tag{3.23}$$

where, k is the isentropic exponent, $q_{V,in}$ is the volumetric flow rate of the gas and P_{in}, P_{out} are the pressure values at the inlet and outlet of the pump, respectively. In this case, the outlet pressure is equal to the atmospheric pressure and thus, equal to 101.3 kPa. In addition, the inlet pressure of the vacuum pump remained constant throughout the experiment and was measured equal to 1500 Pa. The isentropic constant k for water vapor is assumed equal to 1.3 [Bannwarth, 2005]. The volumetric gas flow rate can be found based on the ideal gas law given in Equation 3.24 .

$$P \times V = n \times R \times T \tag{3.24}$$

where P, V and T are the pressure, volume and temperature of the permeate, respectively. R is the ideal gas constant and is equal to 8.314 J/mol/K, and n is the molar flow rate of the water vapor. The water vapor temperature is assumed to remain constant at 50^oC before condensation. A mass balance during the VMD concentration experiment showed that around 10% of the water vapor was not caught by the cool trap. This deviation in the mass balance has been considered as reasonable, taking into account the non-condensable gases and the water that remained in the tubing of the system throughout the experiment. Therefore, for the volumetric gas flow rate, the term n_c=10% will be introduced, which describes the portion of the water vapor and the non-condensable gases that did not end up in the cool trap. The remaining 90% of the gases was collected in the cool trap and hence, not considered in the energy calculations of the vacuum pump.

In Table 3.10, a summary of all parameters that will be used for the calculation of the different energy terms, is provided. Based on the experimental data, the energy requirements of the vacuum pump, cooler and feed recirculation will be then calculated.

Therefore, the energy calculations will estimate the total energy that is required for each recovery stage and concentration factor. The total energy was normalized for the permeate production and for the feed water treated, as well.

Table 3.10: Summary of the parameters assumed, calculated and taken from literature which will be used for the energy calculations of E_2 feed re-circulation, E_3 vacuum pump operation and E_4 operation of cool trap

Energy Terms	Experimentally determined & Calculated	Assumed & Taken from literature	References
E_2	$T = 50^oC$ ΔP=0.5 bar V_f=28.5 l/h	ϵ_{pl}=0.8	Xie et al. [2016]
E_3	P_{out}=101.3 KPa P_{in}=1500 Pa $n_c = 0.10$ A=34 cm^2	$\eta_S = 0.7$ k=1.3	Allen [2009] Bannwarth [2005]
E_4	$P_{out} = 101.3KPa$ $P_{in} = 1500Pa$	$T_{\text{water vapor}} = 50^oC$ $T_{\text{saturated}} = 13^oC$ $\lambda = 2470.06KJ/Kg$ $C_{p,g} = 1.87KJ/Kg/K$ $COP = 4$	Wagner and Pruß [2002] Wagner and Pruß [2002] Vestfálová and Šafařík [2016] da Silva Pereira et al. [2015]

3.10 CHAPTER SUMMARY

The hydrolysate solution provided by Avantium, contains 1 wt % C5/C6 monomeric sugars, 0.5 wt % sugar degradation by-products and 1.6 wt % NaCl. The hydrolysate solution is expected to also contain bigger molecules (e.g., humins or/and soluble lignin) and metal ions. Four (4) tubular ceramic and polymeric NF membranes and one (1) flat sheet MD membrane will be assessed based on their performance in C5/C6 sugar rejection and permeation of NaCl. The sugar concentration goal will be achieved according to a water recovery of 90% of the initial feed solution with a final concentration of 10 wt % of C5/C6 sugars in the concentrate stream. Turbulent hydraulic conditions will be applied for both technologies and calculations of the CF and MTC of the membranes will be used to assess their performance. The NF and VMD will be tested for their water permeability and their performance in C5/C6 sugars & NaCl rejection, first with synthetic feed solutions and finally with the real hydrolysate solution. Pore radius experiments based on the DSPM model will give an insight on the NF membrane characteristics. Surface tension and contact angle measurements will be conducted to investigate the characteristics of the MD membrane and its interaction with the solutes in the hydrolysate solution. Finally, energy calculations for the VMD including two different scenarios for the efficiency of the chiller will offer an indication on the energy consumption of the aforementioned unit.

4 RESULTS AND DISCUSSION

In this chapter, the results from the experimental procedures with the NF and MD set-ups are presented and discussed. In Section 4.1, the results for the tubular NF experiments are analyzed gradually, starting with the water permeability of the NF membranes and closing with the rejection of C5/C6 sugars and NaCl, according to different feed water solutions. The results of the fouling investigation and pore radius calculations of the tubular NF membranes are given in Sections 4.1.5 and 4.1.6, respectively. In Section 4.2 the experimental results of the VMD set-up are described. The water permeability results of the MD membrane are given first, followed by the MD performance in the rejection of C5/C6 sugars and salt, based on different feed temperature gradients. Section 4.2.2 deals with the results from the concentration experiment with (i) synthetic C5/C6 sugars & salt solution and (ii) hydrolysate solution. In the following Section 4.2.3, the MD membrane is tested for its membrane wetting potential based on surface tension and contact angle measurements. The energy consumption of the VMD unit is given in Section 4.2.4, in which the VMD is also compared with literature findings of different concentration technologies.

4.1 NANOFILTRATION EXPERIMENTS

4.1.1 Water permeability

In Figure 4.1, the permeability tests of the tubular NF membranes can be seen, normalised per applied pressure. The permeability was measured by increasing the pressure in the system, where an increase in the flux along with the pressure was observed. The bars in the Figure 4.1 represent the average value of at least triplicate measurements, whereas the error bars are the standard deviations for each NF membrane tested. The most permeable tubular membrane was the 450 Da ceramic membrane as expected from the bigger MWCO in comparison with the other membranes. After the 450 Da, the 200 Da ceramic followed and then, with almost half the permeability, the AFC40 and AFC30 polymeric tubular membranes.

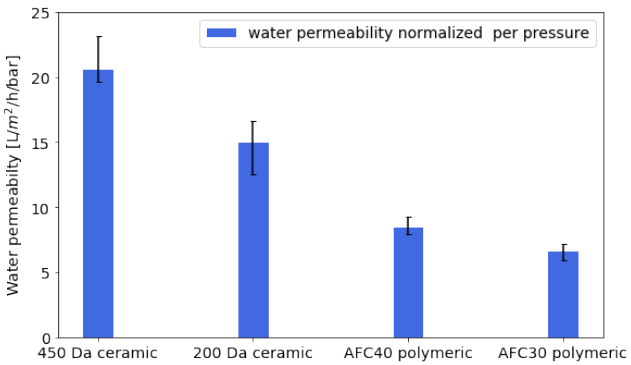

Fig. 4.1: Comparison in the water permeability of the different tubular nanofiltration membranes

4.1.2 Salt rejection

In Figure 4.2, the NaCl rejection of the different tubular NF membranes is depicted. The NaCl rejection values were measured for 10, 30 and 50 LMH, using electrical conductivity (EC) measurements in the feed and permeate streams. The calculations were made based on a calibration line for the EC and NaCl concentration. The bars in Figure 4.2, represent the average value of triplicate measurements, whereas the error bars are the standard deviations for each NF membrane tested. It can be observed that the lowest NaCl rejection was measured in the case of the ceramic tubular membranes, with NaCl rejection in the range of 1-3% for both ceramic membranes. In the case of the 450 Da ceramic membrane, there was no data for the NaCl rejection for 10 LMH of permeate flux, as the system could not operate in the lower pressures.

According to Figure 4.2, it can also be observed that the NaCl rejection of the membranes increased along with the pressure increase. In the case of polymeric membranes, for the AFC40 and AFC30 membranes, the NaCl rejection was in the range of 6-12 % and 8-16%, respectively. The higher NaCl rejection for the polymeric membranes can be justified from their permeability results, as these membranes were proven to be less permeable than the ceramic membranes.

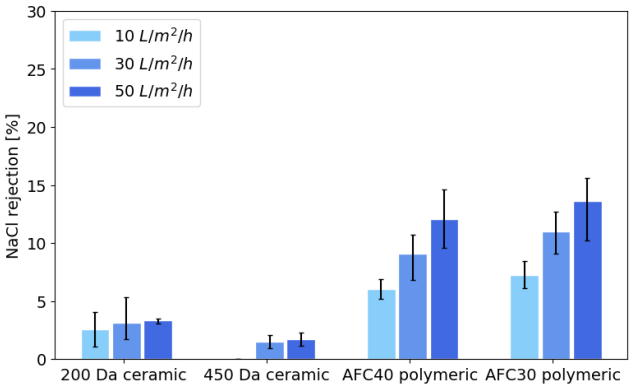

Fig. 4.2: NaCl rejection of the different tubular nanofiltration membranes

4.1.3 Sugar rejection

Synthetic sugar solutions were prepared by adding 1.5 wt % of glucose and xylose separately and mixing each sugar solution with 1.4 wt % NaCl, in demineralised water. The purpose of the synthetic solutions was to determine the rejection of each monomeric sugar by the different NF membranes along with the presence of NaCl, before testing the hydrolysate solution. The results of the glucose rejection for the different membranes can be seen in Figure 4.3. The glucose rejection increased along with the pressure increase for all membranes tested. In Figure 4.3, the bars represent the COD values measured with the photo-spectrometer and the error bars are the standard deviations from these measurements within a range of 10%, as indicated by the machine. The lowest glucose rejection was found for the 450 Da ceramic membrane with a maximum value of 13% for 50 LMH. The glucose rejection for the 200 Da ceramic membrane was almost stable at 32%. The polymeric membranes performed better in terms of glucose rejection with values in the range of 44-63 % and 53-67 % for the AFC40 and AFC30 polymeric membranes, respectively.

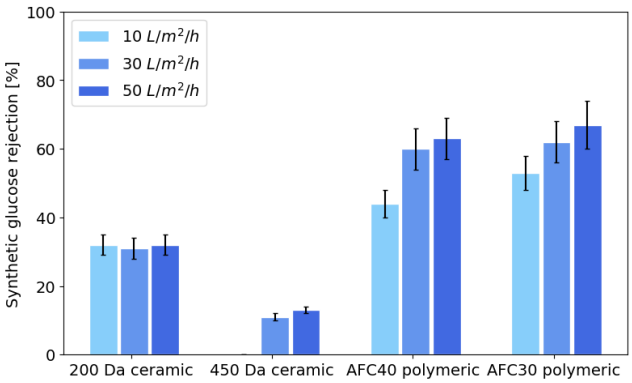

Fig. 4.3: Glucose rejection of the different tubular nanofiltration membranes

The rejection of xylose for the different NF membranes can be seen in Figure 4.4. As in the case of glucose rejection, the membranes performed in the same order in this case as well. The lowest xylose rejection was detected for the 450 Da membrane in the range of 0.2-10%. The 200 Da ceramic membrane rejected xylose in the range of 19-23 % and in the case of polymeric membranes, the range of xylose rejection was 32-45 % and 32-54 % for the AFC40 and AFC30, respectively. The lower rejection in the case of xylose can be explained by its lower MW (150 g/mol) when compared to glucose (180 g/mol). An increased xylose rejection with an increase in the applied pressure can be observed in this case, as well. Overall, it can be deduced that the sugar rejection of all NF membranes was rather low for the sugar concentration purposes of the current study. To further investigate and explain the rejection results, pore radius experiments were conducted for all membranes in this study, according to the methodology mentioned in Section 3.6.

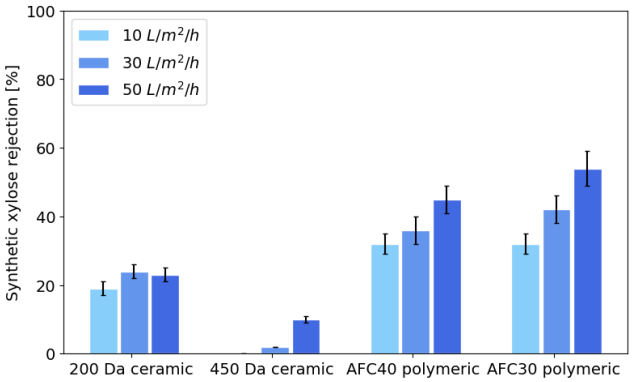

Fig. 4.4: Xylose rejection of the different tubular nanofiltration membranes

4.1.4 Performance of the tubular NF membranes with the hydrolysate solution

To examine the influence of the sugar mixture and the presence of by-products on the sugar rejection of the tubular NF membranes, experiments with the real hydrolysate solution were also conducted. Initially, the results were assessed by measuring the COD rejection values in the permeate samples and afterwards, the permeate and feed samples were further analysed for their concentration in sugars and by-products in Avantium, with IC and HPLC analysis.

The COD rejection values for the NF membranes can be seen in Figure 4.5. As expected from the previous synthetic solution experiments, the AFC40 and AFC30 polymeric membranes had the highest rejection values with a rejection of 74 and 76 % at 50 LMH, respectively. For the ceramic membranes, the highest COD rejection was 61 % for the 200 Da membrane and 33% for the 450 Da membrane. The higher rejection values in this

case can be explained by the rejection of by-products which contribute to the COD values measured.

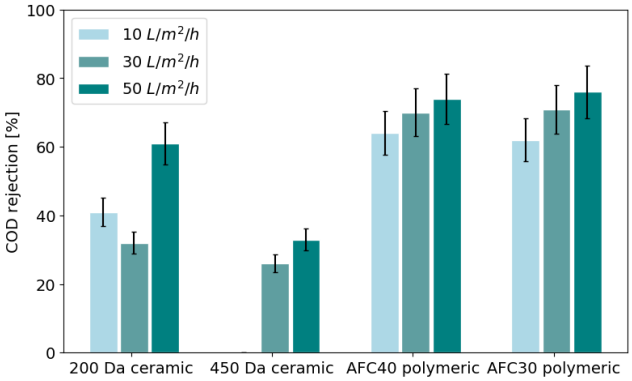

Fig. 4.5: COD rejection of the different tubular nanofiltration membranes using the hydrolysate solution

The actual rejection of C5/C6 sugars can be seen in Figure 4.6. In this case, the overall C5/C6 sugar rejection is depicted, including the sum of the monomeric sugars in the feed water. Interestingly, the C5/C6 sugar rejection was higher than what was measured in synthetic solutions. More specifically, in the case of polymeric membranes, the highest sugar rejection was measured in the case of the polymeric membranes with values of 72 and 81 % for the AFC40 and AFC30, respectively. In the ceramic membranes, an increased rejection was also observed with highest rejection values of 46% and 22% for the 200 Da and 450 Da membranes, respectively. Figure 4.7, shows the rejection of by-products with the tested NF membranes. It can be seen that in the case of the polymeric membranes and the 200 Da the rejection was almost the same with the highest rejection value of around 50%. In the case of the 450 Da membrane, the highest by-products rejection was 24 %. Overall, the increase in the C5/C6 sugar and salt rejection and the decreased water flux can be attributed to the presence of by-products in the hydrolysate solution. The comparative graphs for the rejection of glucose and xylose in the case of synthetic and hydrolysate solutions can be seen in Figure 4.8. The flux decrease for all NF membranes with the hydrolysate solution can be seen in Figure 4.9a. Additionally, the increased salt rejection in the hydrolysate solution experiments can be seen in Figure 4.9b.

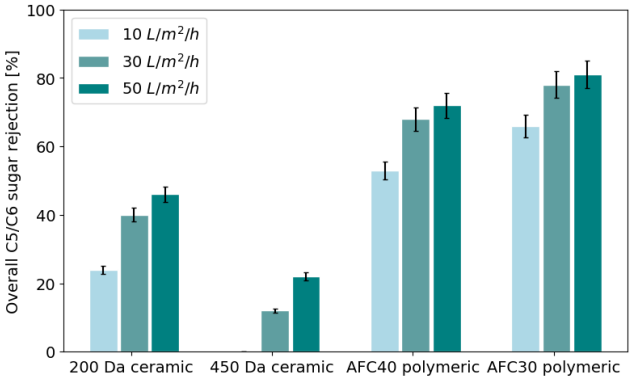

Fig. 4.6: Overall C5/C6 sugar rejection of the different tubular nanofiltration membranes using the hydrolysate solution

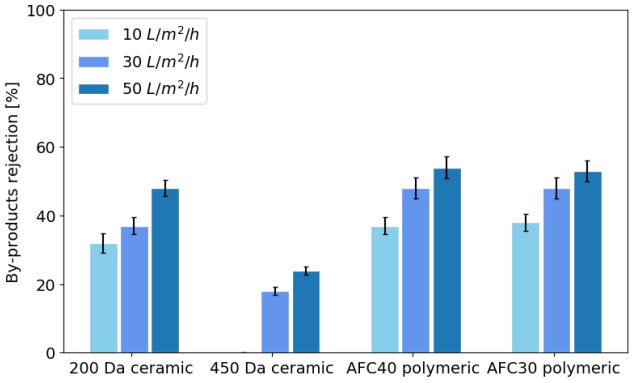

Fig. 4.7: Overall rejection of by-products for the different tubular nanofiltration membranes using the hydrolysate solution

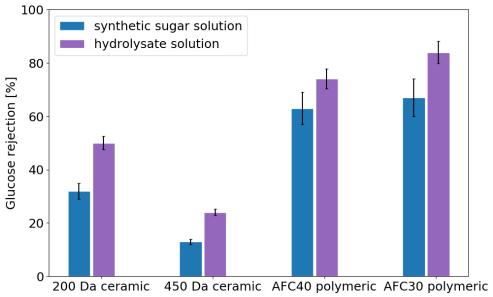

(a) Comparison of glucose rejection between synthetic and hydrolysate solutions for different nanofiltration membranes

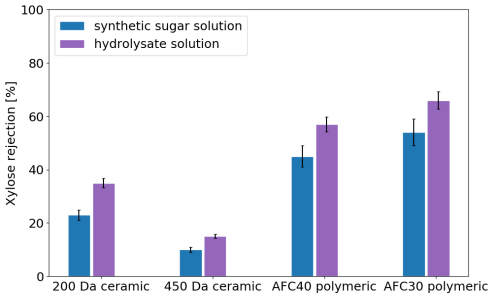

(b) Comparison of xylose rejection between synthetic and hydrolysate solutions for different nanofiltration membranes

Fig. 4.8: Comparison of the C5/C6 sugar rejection with synthetic and hydrolysate solutions

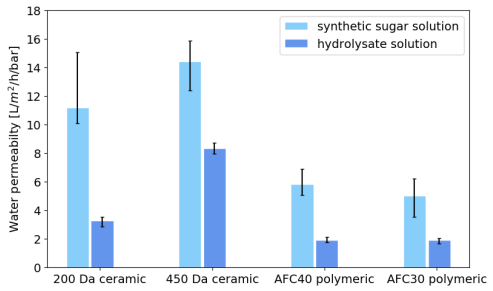

(a) Water permeability comparison using synthetic and hydrolysate solutions as feed water

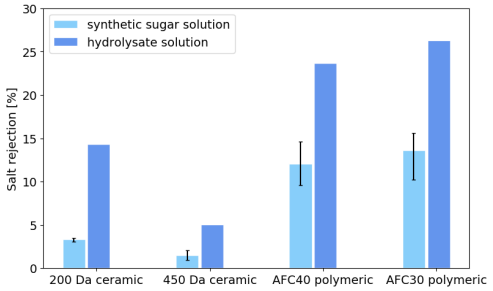

(b) Maximum salt rejection comparison using synthetic and hydrolysate solutions as feed water

Fig. 4.9: Comparison in permeability and salt rejection with synthetic and hydrolysate solutions

4.1.5 Fouling investigation of tubular Nanofiltration membranes

The initial permeability of the NF membranes can be seen in Figure 4.1. Upon the completion of the experiments including the tests with the hydrolysate solution, the membrane system was chemically cleaned with the recirculation of an alkaline solution containing NaOH, and then rinsed thoroughly with demineralized water. Afterwards, permeability tests were performed to investigate the flux recovery of the membranes and the fouling potential and cleaning efficiency. The results from the permeability tests can be seen in

Figure 4.10. As it can be seen from Figures 4.10b and 4.10d, the flux for the 450 Da ceramic and AFC30 polymeric seems to be completely recovered after the cleaning in place (CIP). In the case of the 200Da ceramic and AFC40 polymeric membrane, a decreasing trend in the flux was observed during the final permeability test. More specifically, the initial and final MTC values of the tubular NF membranes can be seen in Table 4.1. According to the MTC values, in the case of the 200 Da and AFC40 NF membranes, there was a flux decrease of 16 and 34 %, respectively. In the case of 450 Da and AFC30, the flux decrease was 4 and 17 %, respectively. Overall, it can be deduced that the ceramic membranes can be efficiently cleaned as in both membranes the flux was successfully restored. In the case of the AFC40 polymeric membrane, the biggest flux decrease was observed, which can be used as an indication for the fouling potential of this membrane. Additionally, from the membrane specifics given in Table 3.4, it can be observed that the maximum pH value for the polymeric membranes is limited to 9.5. Therefore, the alkaline NaOH solution might not be very effective in the cleaning of polymeric membranes. The pH range was not a limiting factor as far as the ceramic membranes are concerned.

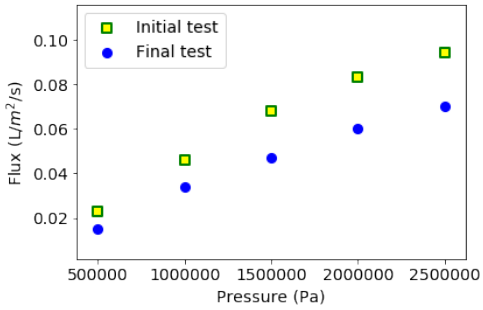

(a) Initial and final permeability test for the 200 Da ceramic membrane

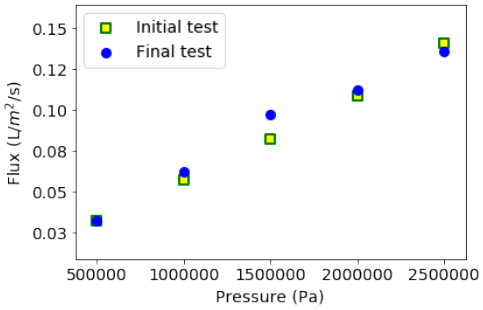

(b) Initial and final permeability test for the 450 Da ceramic membrane

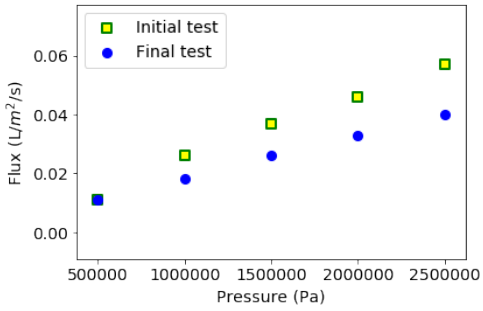

(c) Initial and final permeability test for the AFC40 polymeric membrane

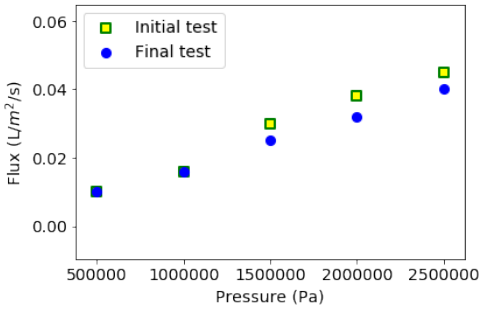

(d) Initial and final permeability test for the AFC30 polymeric membrane

Fig. 4.10: Initial and final permeability tests for the tubular nanofiltration membranes, before and after chemical cleaning

Table 4.1: Initial and final mass transfer coefficient values of the tubular nanofiltration membranes

Mass transfer coefficient [$\times 10^{-8}$ s/m]			
Membrane	Initial value	Final value	Relative difference
450 Da ceramic	5.39	5.18	4%
200 Da ceramic	3.24	2.72	16%
AFC40 polymeric	2.23	1.48	17%
AFC30 polymeric	1.82	1.51	34%

4.1.6 Pore radius calculations

The results for the pore radius of the 200 & 450 Da ceramic and AFC40 & AFC30 polymeric membranes can be seen in Figures 4.11, 4.12, 4.13 and 4.14 respectively. Each sugar solute was fitted to its theoretical rejection and yielded a different pore radius for each tested membrane. The rejection measurements for each solute were made based on the COD (mg/L) values derived from the photo-spectrometer. The error bars represent a standard deviation within 10% from the value measured. Based on the values found for each sugar solute and membrane, an average pore size was calculated. More specifically, the pore radius from the minimised sum squared errors for each solute can be seen in Table 4.2, along with the calculated average pore radius of each membrane.

As expected, the membrane with the biggest pore size was found to be the 450 Da ceramic, with an average pore size of 2.17 nm. When compared with the pore size given by the manufacturer (Table 3.3), it can be seen that the calculated value is almost 2.5 times bigger. The average pore radius of the 200Da ceramic was calculated to be 1.78 nm and was found to be close to the pore radius of the 450 Da membrane. This finding can be also supported by the low C5/C6 sugar rejection values of the 200 Da ceramic membrane, which were close to those of the 450 Da. For the polymeric membranes, no specifications were provided by the manufacturer. The average pore radius of the AFC40 and AFC30 polymeric membranes was calculated to be 0.64 and 0.62 nm, respectively, which is almost 50 % lower in size than in the case of ceramic membranes. The calculated pore radius for the polymeric membranes is in line with the rejection values measured for these membranes. Additionally, the pore radius of the AFC30 membrane is the smallest one, which can be supported by its highest C5/C6 sugar rejection values. The similar C5/C6 sugar rejection values for the polymeric membranes can be supported by the similar calculated pore radius. Furthermore, based on the Stokes radii of the sugar solutes (see Table 3.8) and the membrane pore size calculated, higher sugar rejection values were not expected for all tested NF membranes as the Stokes radii of all sugar solutes is smaller than the smallest calculated pore size.

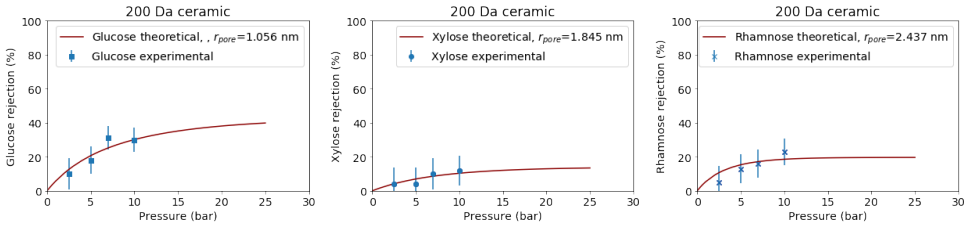

(a) Pore radius for the 200 Da ceramic membrane using glucose

(b) Pore radius for the 200 Da ceramic membrane using xylose

(c) Pore radius for the 200 Da ceramic membrane using rhamnose

Fig. 4.11: Pore radius calculations for the 200 Da ceramic membrane

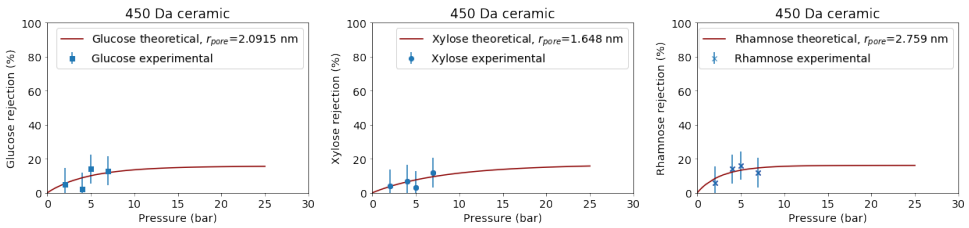

(a) Pore radius for the 450 Da ceramic membrane using glucose

(b) Pore radius for the 450 Da ceramic membrane using xylose

(c) Pore radius for the 450 Da ceramic membrane using rhamnose

Fig. 4.12: Pore radius calculations for the 450 Da ceramic membrane

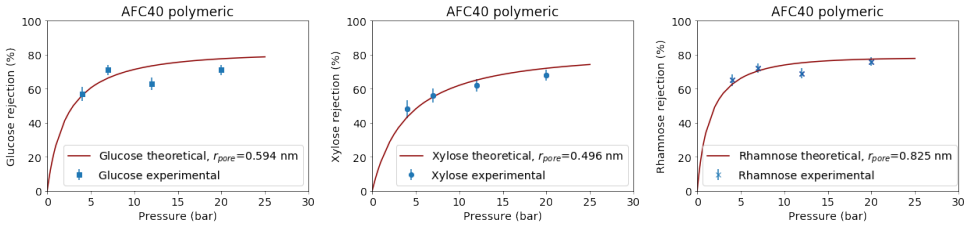

(a) Pore radius for the AFC40 polymeric membrane using glucose

(b) Pore radius for the AFC40 polymeric membrane using xylose

(c) Pore radius for the AFC40 polymeric membrane using rhamnose

Fig. 4.13: Pore radius calculations for the AFC40 polymeric ceramic membrane

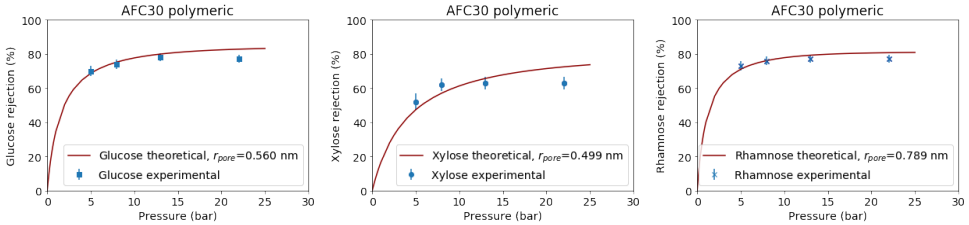

(a) Pore radius for the AFC30 polymeric membrane using glucose

(b) Pore radius for the AFC30 polymeric membrane using xylose

(c) Pore radius for the AFC30 polymeric membrane using rhamnose

Fig. 4.14: Pore radius calculations for the AFC30 polymeric ceramic membrane

Table 4.2: Pore radii calculated for different solutes and NF membranes and average pore radius of each membrane

Pore radii (r_p) in nm				
Membrane	Glucose	Xylose	Rhamnose	Average r_p
200 Da ceramic	1.056	1.845	2.437	1.779
450 Da ceramic	2.092	1.648	2.759	2.166
AFC40 polymeric	0.594	0.496	0.825	0.638
AFC30 polymeric	0.560	0.499	0.789	0.616

4.2 MEMBRANE DISTILLATION EXPERIMENTS

4.2.1 Permeability and solute rejection

The water flux and the sugar & salt rejection for the 0.2 μm MD membrane was investigated for three different temperatures of 40, 45 and 50 ^{o} C. Due to the prior hydrolysis and the assumption that the feed temperature will be held stable at 50 ^{o} C , the influence of a 10^{o} C drop in the feed temperature on the flux and sugar and salt rejection, was investigated. Figure 4.15 depicts the flux of the VMD set-up according to different applied temperature gradients and types of solution. The bars represent the average values of triplicate measurements and the error bars the minimum and maximum values of these measurements. As it can be seen, there was a flux increase in correlation with the increase in the driving force. The highest flux was achieved during the permeability tests with the demineralized water, whereas for the rest of the solutions tested, a flux *decrease* was observed. In Table 4.3 the MTC of the MD membrane is presented for the average water flux measured and according to different applied feed temperatures. A decrease in the calculated MTC values was observed with the increase in the feed temperature. The latter means that the membrane was less permeable with an increase in the feed temperature. This observation can be attributed to the temperature polarisation phenomena during the VMD operation.

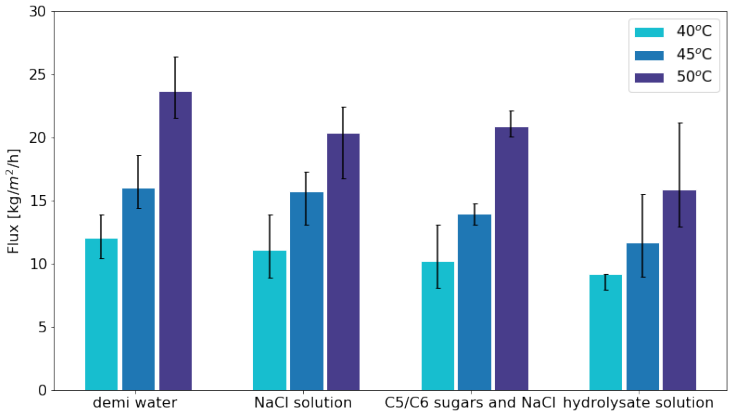

Fig. 4.15: Flux evolution with an increase in the applied temperature and for the different solutions

Table 4.3: Mass transfer coefficient of MD membrane at different feed temperature

Mass transfer Coefficient for the MD membrane	
Temperature [^{o}C]	MTC [x 10^{-6} s/m]
40	1.27
45	1.07
50	1.02

More specifically, in the case of the synthetic solutions with NaCl and the C5/C6 sugars, it can be witnessed that there was a flux decrease of 13 % in comparison with the demineralized water. The synthetic solutions were made gradually by adding first the NaCl and then the C5/C6 sugars to investigate the influence of every parameter in the salt & sugar rejection of the membrane and in the water flux as well. From the different synthetic solution experiments, it was observed that the presence of sugars in the NaCl solution did not have a great impact on the water flux decrease, in comparison with the solution containing solely NaCl. The biggest flux decrease can be seen in the case of the hydrolysate solution, as the flux was measured to be approximately 23% lower than the flux measured with demineralized water. Therefore, the *presence of by-products* seemed

to have an impact on the water flux and thus, to *hinder the water permeation.*

Figure 4.16a, depicts the COD rejection measured at different temperature gradients for both synthetic and hydrolysate solutions. The bars here represent the values measured with the spectrophotometer and the error bars the standard deviations that lie within 10%. As it can be observed in Figure 4.16a, in the case of the synthetic C5/C6 sugar mixture, the sugar rejection was 100% for all temperature gradients. Regarding the hydrolysate solution, the COD rejection was lower and in the range of 70-80 %. The presence of volatile sugar degradation products and hence, their transport in the permeate stream, led to these variations in the COD rejection of the MD membrane. The salt rejection for all cases and solutions was >99 % (Figure 4.16b). Based on the biggest flux production in the case of the hydrolysate solution and the complete sugar rejection at all temperature values, two different sugar concentration tests were conducted at 50 ^oC; one using a synthetic C5/C6 sugar and NaCl solution and a second one, using the real hydrolysate solution.

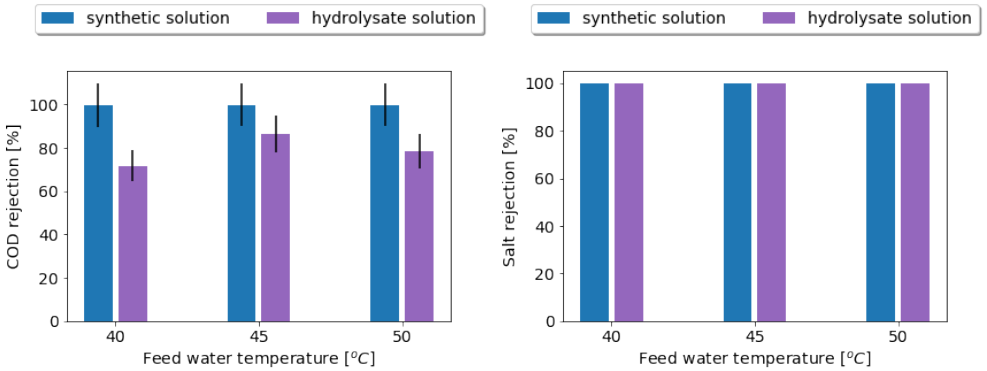

(a) COD rejection of the MD membrane for both synthetic C5/C6 sugar mixture & NaCl and hydrolysate solution, for different applied feed temperatures

(b) Salt rejection of the MD membrane for both synthetic C5/C6 sugar mixture & NaCl and hydrolysate solution, for different applied feed temperature values

Fig. 4.16: Salt and COD rejection of the Membrane Distillation membrane for both synthetic C5/C6 sugar mixture & NaCl and hydrolysate solution, for different applied feed temperature values

4.2.2 Concentrating the C5/C6 sugars

Two C5/C6 sugar concentration experiments were conducted using (i) a synthetic sugar & salt solution and (ii) the real hydrolysate solution. A mixture of C5/C6 monomeric sugars and NaCl was used for the synthetic sugar concentration experiment. The initial concentration of C5/C6 sugars and NaCl was 1.3 wt % and 1.5 wt %, respectively. The feed temperature was held stable at 50^oC for both concentration experiments. During the concentration experiments, feed samples were taken at different time intervals to determine the water recovery and the CF of NaCl and C5/C6 sugars. The experimental duration for the different recovery values was not continuous. After each experimental run, the feed pump was stopped and the set-up was left overnight. The permeate and feed samples were kept in the fridge. Following the completion of each experimental run, the mass of the permeate water that was collected in the distillate flasks, was weighted and analysed for COD and NaCl concentration.

In Figure 4.17, the water flux in correlation with the water recovery is presented for both solutions. The dots and triangles represent the average flux measured at the end of each experimental run. Throughout the concentration experiments, the water flux shows a *decreasing trend* along with the increase in the recovery values. This observation has to

do with the increase in the solute concentration which hinders the water permeation. The water flux regarding the synthetic solution and the water recovery of 86 % , was measured to be 32% lower. At the end of the concentration experiment with the *synthetic solution*,

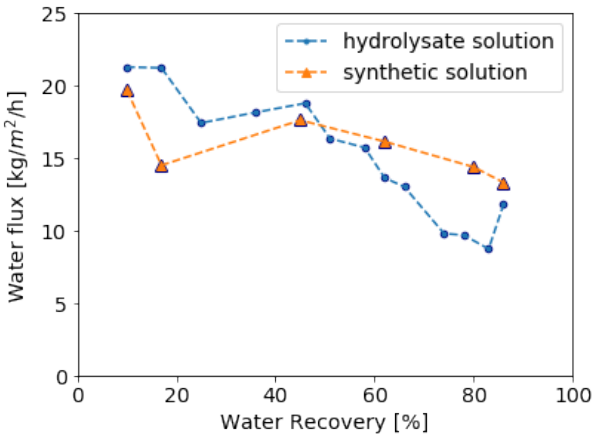

Fig. 4.17: Flux comparison at different recovery values for synthetic and hydrolysate solutions

the system was rinsed with demineralized water and the water flux was measured again, where *no decrease in the water flux* was observed in comparison with the previous permeability tests. As far as the *hydrolysate solution* is concerned, a decreasing trend can also be observed for the water flux along with the increasing concentration of sugars and salt. The *decrease in the flux* after the 50% recovery was *steeper* in the case of the hydrolysate solution. The presence of by-products and their partial concentration can justify the lower fluxes achieved in the concentration experiment with the real hydrolysate water. Additionally, an increase in the water flux can be observed in the water recovery range of 80-86 % in the case of the hydrolysate solution. Before the last recovery stage of 86 % the VMD set-up was not operated for more than 48 hours and therefore, it was rinsed with demineralized water to prevent bio-fouling in the system. Consequently, this increase in the flux can be attributed to the partial cleaning of the membrane.

The concentration factors of C5/C6 sugars and NaCl can be seen in Figure 4.18, in correspondence with the recovery values achieved, for the synthetic solution tests. As it can be observed, the CF of the C5/C6 sugars in the synthetic solution was in accordance with the achieved recovery throughout the experiment. The maximum concentration factor achieved for the C5/C6 sugars was almost 8. A water recovery of 86% and a sugar rejection of >99% would lead to a sugar CF of 7.14. However, the CF for the C5/C6 sugars was calculated to be higher than 7.14 according to both IC and COD analyses. This difference in the calculated CF can be attributed to the balance errors during the mass logging and to the deviations in the COD and IC measurements. According to the >99% NaCl rejection, the same trend would be expected for the CF of NaCl. However, as it can be seen in the graph, at the recovery value of 86% the CF of NaCl was around 4.5 based on the EC measurements. The difference in the CF of NaCl can be explained by the EC measurements at high salt concentrations. A calibration curve for NaCl and EC showed that the EC is not linearly correlated with the NaCl concentration as far as high salt concentrations are concerned. While the NaCl concentration in the permeate water was measured at very low EC values after each experimental run, at the recovery of 86 % the EC was measured around 1.7 mS/cm, which is a high value considering the EC of very pure water (40 μS/cm). In Figure 4.19, the *COD and EC* measurements in the *distillate* water are presented in the case of the *synthetic solution*. An *increasing trend* along with the recovery increase was witnessed for both measured values and more specifically after the water recovery of 50 %. At the recovery stage of 86 % there was a steep increase of the COD detected in the distillate and the biggest value for the EC. These measurements are

indicative for membrane wetting, as low measured values were expected for both EC and COD in the distillate. To further investigate if sugars had passed in the distillate, samples at the recovery values of 80 and 86 % were sent to Avantium for IC analysis, where 0.1 and 0.8 g/L of C5/C6 sugars were measured in total, respectively. However, the analysis of feed water and concentrate water after 86% recovery, verified the CF of 8 calculated based on the COD analysis.

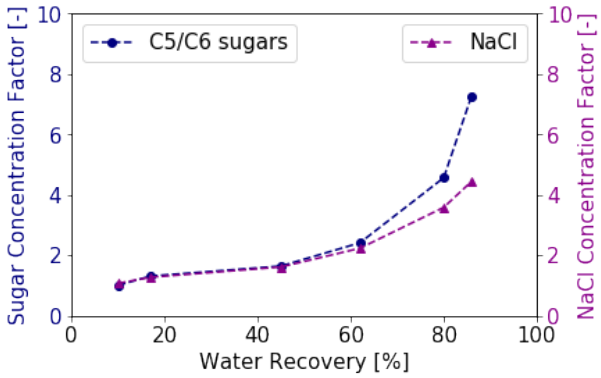

Fig. 4.18: Salt and sugar concentration values at each recovery stage for the synthetic solution

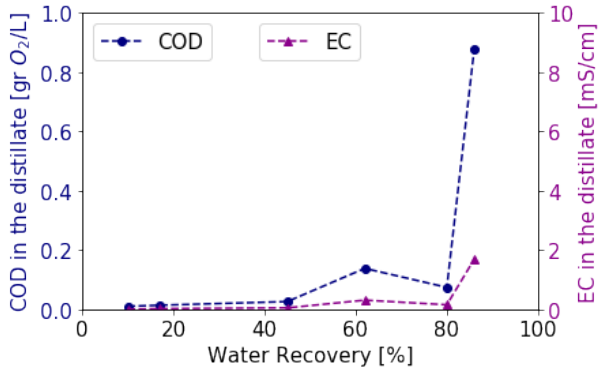

Fig. 4.19: COD & NaCl concentration in the distillate at each recovery stage for the synthetic solution

For the C5/C6 sugar concentration test using the real *hydrolysate solution*, the COD rejection at different recovery stages can be seen in Figure 4.20. The *COD rejection* of the MD membrane was *increased* along with the increasing recovery. That can be justified from the transport of the volatile by-products throughout the concentration experiment. After the recovery stage of 60 %, the COD rejection seems to stabilize and reach rejection values of approximately 100 %. In Figure 4.21, the actual concentration of the C5/C6 sugars in the concentrate stream is depicted, along with the salt concentration in the case of the hydrolysate water. The analysis of the concentrate samples has been done with IC analysis by Avantium. As it can be seen, an increasing trend in the overall C5/C6 sugar concentration and in the salt concentration was observed. The *decreasing transport of the volatile by-products* with the increase in the water recovery, can also be observed in Figure 4.22, in which the COD and the EC measurements in the distillate are presented. According to these measurements a decrease in the COD values of the distillate was detected, after the water recovery of 60%. Therefore, it can be deduced that most of the volatile by-products have been transferred to the distillate during the previous water recovery stages. The CF for the C5/C6 sugars was >6 and for the salt >4, respectively. The

values for the EC in the distillate also followed an increasing trend (Figure 4.22), however the conductivity in the distillate stayed in low values. An IC analysis of the distillate showed that there was *no detectable transport of C5/C6 sugars* in the collected permeate samples. The CF of salt and sugars followed a very similar trend for both concentration experiment (Figures 4.23 & 4.24).

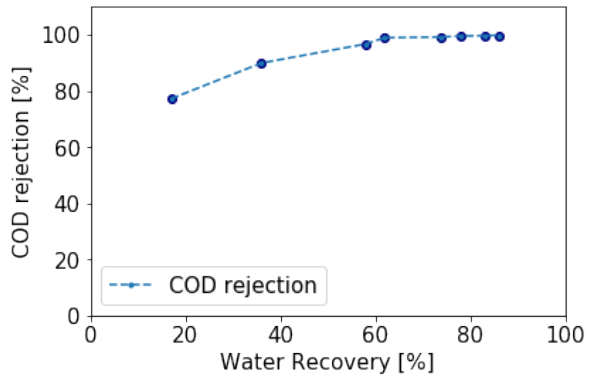

Fig. 4.20: COD rejection for the hydrolysate solution at each recovery stage throughout the experiment

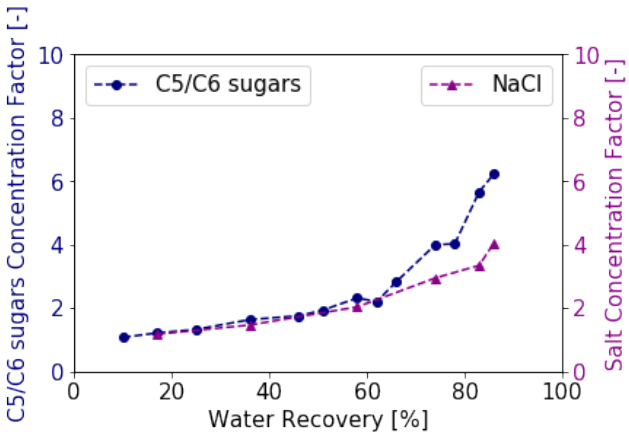

Fig. 4.21: Salt and sugar concentration values at each recovery stage for the hydrolysate solution

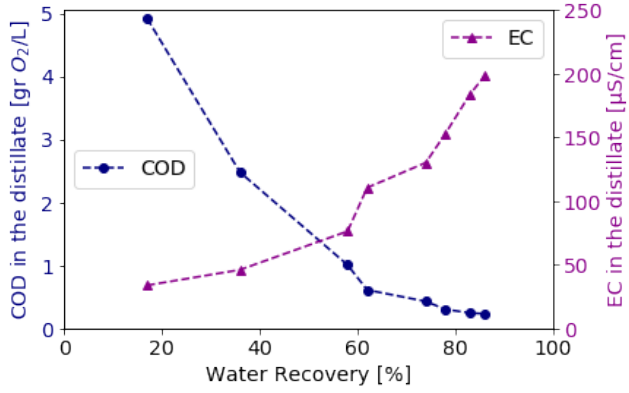

Fig. 4.22: COD & salt concentration in the distillate at each recovery stage for the hydrolysate solution

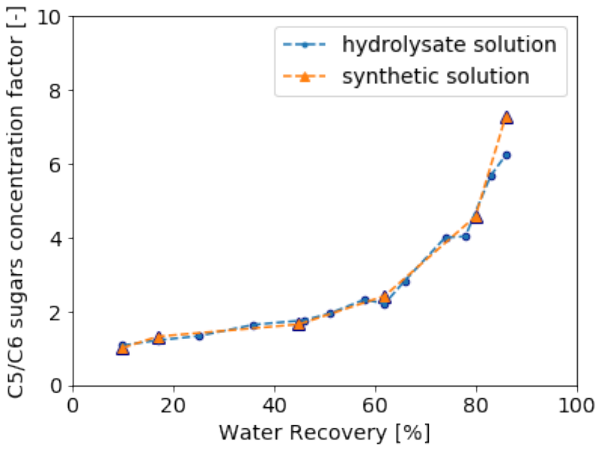

Fig. 4.23: C5/C6 sugar concentration factor comparison at different recovery values for synthetic and hydrolysate solutions

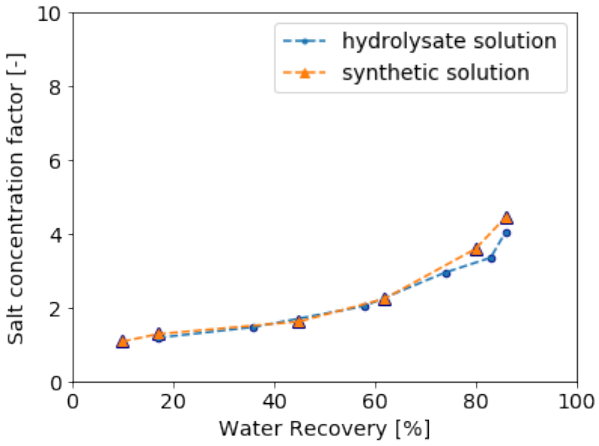

Fig. 4.24: Salt concentration factor comparison at different recovery values for synthetic and hydrolysate solutions

Upon the completion of the concentration experiment with the hydrolysate solution, the system was cleaned with a NaOH solution with a pH of 12 and afterwards, thoroughly rinsed with demineralized water. Following the cleaning, the membrane stayed immersed in demineralized water for 1 hr and eventually was left to dry in atmospheric air, according to the instructions of the manufacturer. The water flux of the MD membrane was measured before and after the concentration experiment and after the CIP, to determine the CIP efficiency and the fouling of the membrane. As it can be seen in Figure 4.25, the water flux was decreased by 50 % after 39 hours of operation with the hydrolysate solution. However, the chemical cleaning with the NaOH solution led to a complete flux recovery. Therefore, it can be deduced that the *fouling* of the hydrophobic MD membrane *is reversible* with the use of chemical cleaning agents and the drying procedure. However, the fouling of the MD membrane as presented in Figure 4.25, could be a problem in full-scale applications, because of the need for frequent membrane cleaning to restore the performance of the membrane. In Figure 4.26, the partial membrane wetting of the PTFE MD membrane is presented as colored droplets on the permeate side, after the treatment of the hydrolysate solution. The cleaning efficiency of the MD membrane before and after the CIP can be seen in Figure 4.27. Figure 4.27 depicts the feed side of the MD membrane after the hydrolysate solution concentration experiment and after the CIP. In Figure 4.27a, it can be observed that the fouling agents of the hydrolysate solution adsorbed on the surface of the membrane and as a result they blocked the membrane pores and contributed to the decreased flux measured. The potential presence of divalent cations (e.g. Ca^{+2}, Mg^{+2})

and organic matter in the hydrolysate water might have enhanced the fouling of the MD membrane due to their interaction, which can result in the formation of complexes that can deposit on the membrane [Bush et al., 2016]. In addition to the organic fouling, the deposition of salts on the surface of the membrane might have also been responsible for the decrease in the permeate flux and for the membrane wetting phenomena observed during the operation. Because the operation of the VMD was not continuous throughout the concentration experiments (>12 hours of no operation after 8 hours of continuous operation), the crystallization of salt might have been promoted on some parts of the membrane's surface, resulting in salt deposits and pore blockage. These deposits could have enhanced the membrane wetting phenomena, as observed in the concentration experiments [Ying Shi et al., 2020]. An ionic composition analysis of the hydrolysate solution is therefore imperative to investigate the scaling tendency of different salts during the VMD operation and the interaction of the metal ions with the other organic components in terms of fouling.

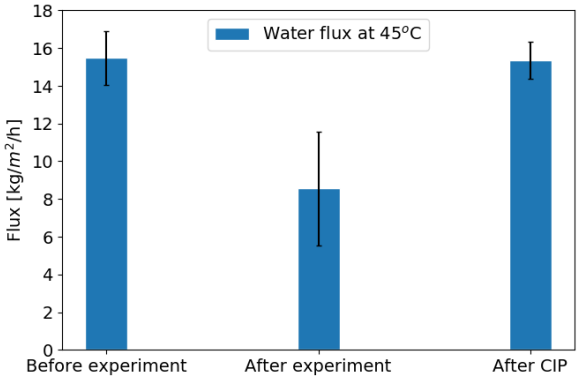

Fig. 4.25: Flux before and after the concentration experiment with the hydrolysate solution and after chemical cleaning

Fig. 4.26: Indication of partial membrane wetting with the appearance of colored droplets on the permeate side of the MD membrane

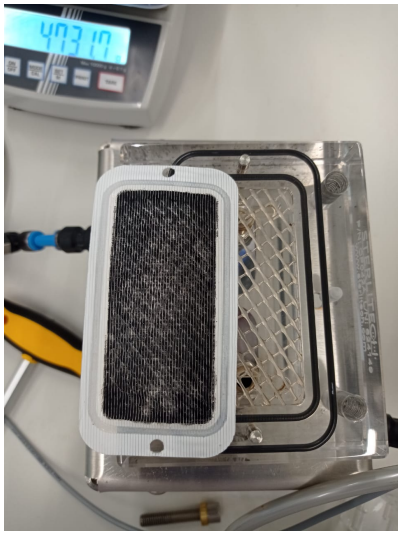

(a) MD membrane after the concentration experiment with the hydrolysate solution

(b) MD membrane after the chemical cleaning and rinsing with demineralized water

Fig. 4.27: Feed side of MD membrane before and after the chemical cleaning upon the completion of the concentration experiment with the hydrolysate solution

According to the results of the synthetic C5/C6 sugar & NaCl solution, membrane wetting was observed, as NaCl and sugars were detected in the distillate samples at high recovery values. Although membrane wetting was also expected in the case of the hydrolysate solution with the appearance of colored droplets, IC measurements for the sugar content of the distillate samples showed otherwise. Further investigation of the membrane wetting phenomena in the MD membrane was conducted with surface tension and contact angle measurements. The results and calculations based on these measurements are presented in the following Section 4.2.3.

4.2.3 Wetting prediction of the MD membrane

Wetting prediction based on surface tension

The contact angle of diiodomethane and demineralized water on the different parts of the PTFE membrane can be seen in Table 4.4. Based on the OWRK model described in Section

Table 4.4: Contact angle measurements of diiodomethane and demineralized water on three different parts of the PTFE MD membrane

Contact angle measurements [^{o}]				
Liquid	$Part_I$	$Part_{II}$	$Part_{III}$	Average
Diiodomethane	39.42	59.92	71.59	56.98
Water	108.38	104.06	112.57	108.34

3.8 and the average contact angle of the two liquids on the PTFE membrane, the surface tension of the membrane was calculated to be equal to 30.55 mN/m. In Figure 4.28, a graph of the surface tension of different hydrolysate samples versus the surface tension of the membrane is presented. The dots represent the values measured with the ring method with a reproducibility of the measurements of around 2%. As it can be seen from the graph, the surface tension of the hydrolysate solution showed some fluctuations along with the increasing recovery. However, the surface tension of all samples was measured to be higher than the calculated surface tension of the membrane. Therefore, no membrane wetting was expected taking into account the surface tension of the liquid and the membrane's surface tension.

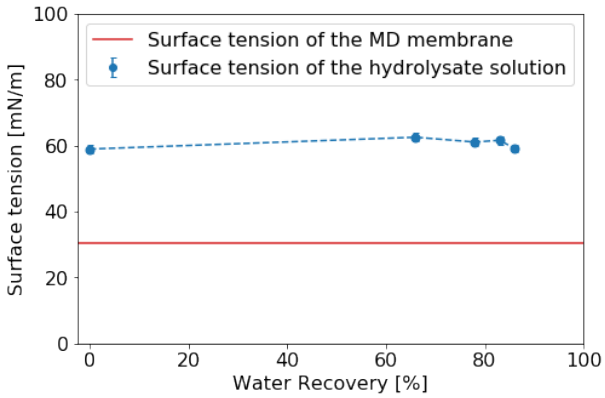

Fig. 4.28: Surface tension of hydrolysate samples at different recovery values versus the calculated surface tension of the PTFE membrane

Wetting prediction based on contact angle measurements

According to the results of the surface tension measurements, no wetting was expected in the case of the current PTFE membrane and concentrated hydrolysate samples. However, during the conduction of the concentration experiment, colored droplets were noticed in the permeate side of the membrane, which led to further investigate the characteristics of the MD membrane. For this purpose, contact angle measurements were performed using different solutions on the PTFE membrane.

More specifically, contact angle measurements of synthetic NaCl and monomeric sugar mix solutions were conducted, following the procedure as described in Section 3.8. The contact angle of the hydrolysate solution at different CFs on the membrane surface was also investigated. The synthetic solutions were tested for different CFs to simulate the concentration experiment with the hydrolysate solution. The goal of the synthetic solution tests was to investigate separately the factors that could have led to the appearance of the colored droplets in the permeate side. For the synthetic solutions, those with a CF of 1 are the starting solutions with a NaCl concentration of 1.5 wt % and a sugar concentration of 1.4 wt %. These values were chosen according to the NaCl and sugar concentration in the real hydrolysate solution. The same synthetic solutions were also tested by increasing the concentration by a factor of seven (CF=7).

The contact angles of the synthetic solutions were measured for three (3) different parts of the membrane's active surface area, whereas for the hydrolysate solution, four (4) different parts were used to obtain more accurate data for the membrane in correlation with the real hydrolysate solution. In Figure 4.29, the average contact angle values of the different synthetic solutions are depicted in a bar chart, including the error bars for the minimum and maximum values that were measured. As it can be seen in Figure 4.29, the synthetic solutions at different concentration values were not expected to cause wetting on the membrane. When the lowest contact angle values on the PFTE membrane are considered, it can be seen that the wetting limit of 90^o (red line) was not reached in any case. With contact angle values lower than 90^o, the liquid droplet is expected to penetrate the porous membrane surface [Franken et al., 1987]. However, that was not the case for the synthetic solutions as the contact angles remained high for both sugar and salt solutions, even in higher concentrations. Furthermore, it can be seen that when sugars were introduced in the solution, the average measured contact angles slightly dropped, however the contact angle values did not change with further sugar concentration. The contact angle and surface tension measurements and a visual representation of the contact angles as given by the instrument apparatus, are provided in Section B.3 of Appendix B.

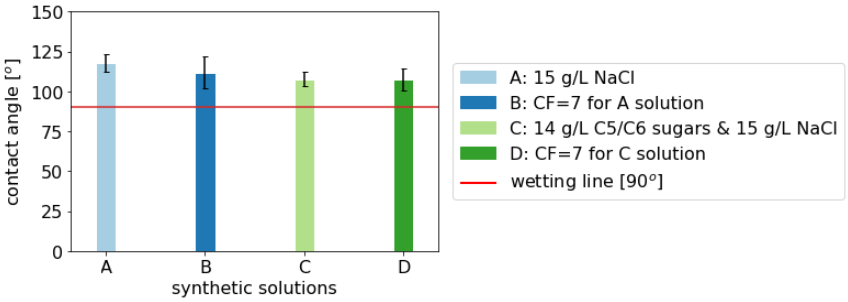

Fig. 4.29: Average contact angle measurements of synthetic solutions on the PTFE MD membrane, at different concentration factors, versus the wetting line of 90^o contact angle

A graph with the measured contact angles using the real hydrolysate solution at different concentration values, can be seen in Figure 4.30. In the graph, the dots represent the average contact angle measured and the error bars the standard deviation (according to the minimum and maximum values measured) for each sample. It can be observed that between the recovery values of 60-80%, the average contact angle of some hydrolysate samples was below the wetting line and thus, wetting of the membrane can be expected. However, this finding is not in agreement with the findings of the surface tension measurements and SFE calculations. Additionally, for both synthetic and hydrolysate solutions, it can be seen that the contact angle values varied for the different parts of the membrane. The variation of the contact angle values on the different parts of the membrane indicated a lower hydrophobicity in some parts of the active surface area of the MD membrane. According to the modified Young Laplace Equation (see Equation 2.1) bigger pore sizes and lower contact angles (decreased hydrophobicity) can both lead to lower LEP values and subsequently, to membrane wetting. The pressure gauges installed in the feed and permeate streams of the VMD set-up ensured that the LEP value of 2.5 bar (as provided by the manufacturer) was not violated throughout the concentration experiments. Taking into account the surface tension values measured for the feed liquid at different CFs, it was deduced that the appearance of colored droplets on the permeate side of the MD membrane was a result of bigger pores and of a lower hydrophobicity in some parts of the MD membrane.

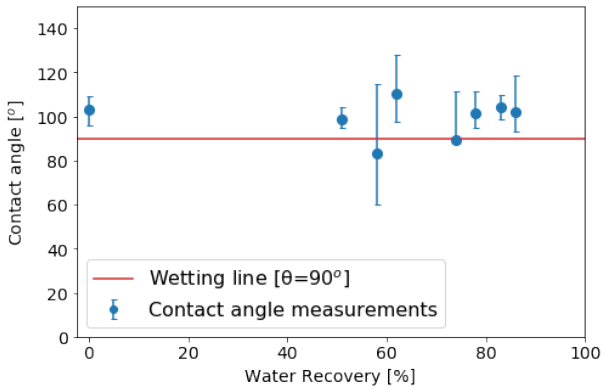

Fig. 4.30: Average contact angle measurements the hydrolysate solution on the PTFE MD membrane, at different recovery values, versus the wetting line of 90^o

4.2.4 Energy calculations

According to the methodology presented in Section 3.9, the following Figures 4.31 & 4.32 display the total energy consumption of the VMD along with the different recovery values and efficiency scenarios for the cooler. As it can be seen in Figure 4.31, the energy consumption at the different recovery stages was normalised according to the permeate production. It can be observed that there was a negligible fluctuation in the energy consumption between the different recovery stages, for both cooler efficiency scenarios. However, a decrease in the energy consumption was observed with an increase in the efficiency of the cooler. More specifically, at 86% recovery, the energy consumption of the VMD in the lab-scale scenario was found to be 736 KWh/m^3 of permeate, whereas in the industrial scenario, the energy consumption was calculated equal with 207 KWh/m^3 for the same recovery.

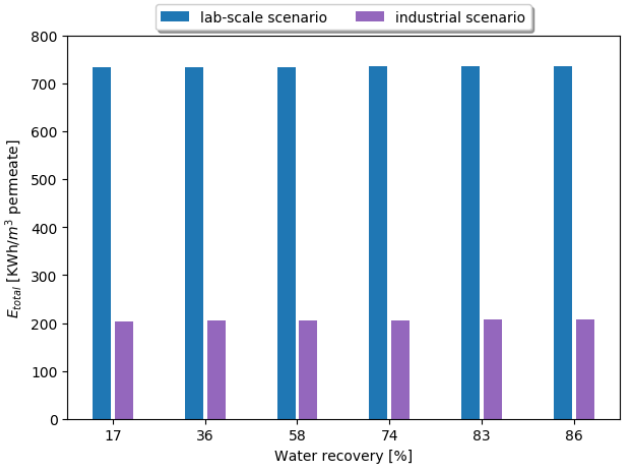

Fig. 4.31: Total energy consumption of VMD, per m^3 of permeate production, at different recovery values and cooler efficiency scenarios

Figure 4.32, depicts the energy consumption of the VMD at different recovery values. However, the total energy consumption in this case was normalized based on the m^3 of feed water treated. It can be observed that the energy consumption increased along with the recovery values, starting at 122 KWh/m^3 at 17% recovery and reaching 630.5 KWh/m^3, at 86% recovery. The impact of the cooler's efficiency on the overall energy consumption can be seen in this case as well, with a decrease of approximately 3.5 times in the VMD energy requirements, when considering the industrial scenario.

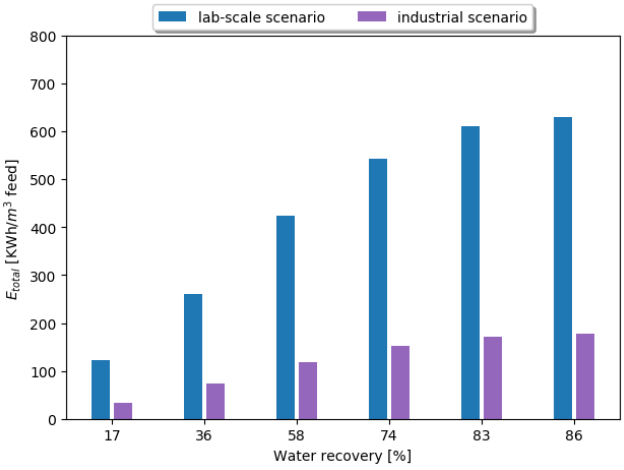

Fig. 4.32: Total energy consumption of VMD, per m^3 of feed water treated, at different recovery values and cooler efficiency scenarios

Ultimately, in Figure 4.33, the contribution of the feed re-circulation, vacuum pump and cooler in the total energy consumption is presented. As it can be deduced from the graph, the cooler was the main contributor to the total energy consumption of the VMD. After the cooler followed the vacuum pump and lastly, the feed recirculation. The latter had a negligible impact on the total energy consumption of the VMD operation. The energy contribution of the aforementioned components for the different recovery values tested, can be seen in Table 4.5. The total consumed energy that is presented in the last two columns of Table 4.5, was normalized per m^3 of permeate production and feed water in Figures 4.31 and 4.32, respectively.

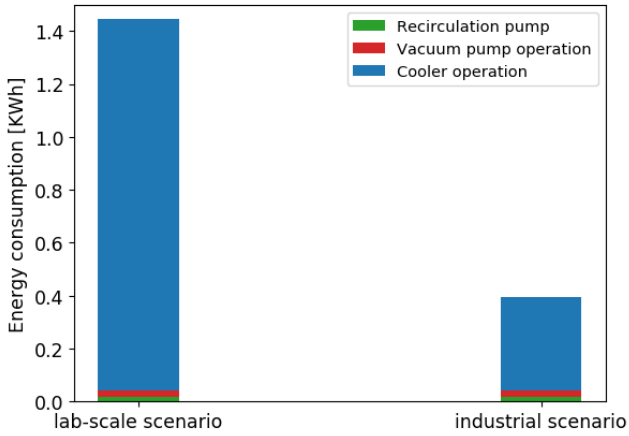

Fig. 4.33: Contribution of the feed re-circulation, vacuum pump and cooler operation to the total energy consumption for both scenarios of the cooler efficiency

Table 4.5: Energy contribution of feed re-circulation (E_2), vacuum pump operation (E_3), operation of cooler E_4 and total energy consumption for the two different efficiency scenarios of the cooler at different recovery values

Calculated energy consumption for the lab-scale experiment [KWh]					
Recovery(%)	E_2	E_3	E_4	$E_{tot/lab-scale}$	$E_{tot/industrial}$
17	0.0026	0.0081	0.2728	0.28	0.079
36	0.0036	0.0093	0.3119	0.32	0.09
58	0.0044	0.0109	0.3649	0.38	0.10
74	0.0044	0.0078	0.2602	0.27	0.07
83	0.0032	0.0046	0.1523	0.16	0.04
86	0.0007	0.0013	0.0427	0.044	0.01
SUM	0.02	0.04	1.41	**1.47**	**0.41**

The calculated energy consumption of the VMD unit can be compared with the energy consumption of the different evaporators presented in Section 2.3. When compared to a singe-effect evaporator, the energy consumption of VMD per kg of permeate production was calculated to be almost 3 times lower (taking into consideration the industrial scenario). However, when compared with multi-effect evaporators, the VMD seems to be a more energy efficient choice only in the case of evaporators with up to three (3) effects. With the addition of more than 3 effects, the energy consumption of an evaporator could be lower than the VMD energy consumption. More specifically, a 6-effect evaporator can have 2 times lower energy consumption than that of VMD. Overall, the VMD appears to be a competitive technology in industrial applications in comparison with contemporary evaporators.

4.3 CHAPTER SUMMARY

According to the results discussed in Chapter 4, the tubular NF membranes were proven not suitable to achieve the C5/C6 sugar concentration goals as a result of their low sugar rejection values. The tested polymeric membranes performed better than the ceramic ones, with a maximum C5/C6 sugar rejection of 81 % in the case of the hydrolysate solution. A maximum C5/C6 sugar rejection increase of 36 % for the ceramic and of 21% for the polymeric membranes, was observed in comparison with the synthetic C5/C6 sugar solution and can be attributed to the presence of sugar by-products in the hydrolysate water. The salt rejection was also increased with the hydrolysate solution, with a maximum rejection increase of 79% for the 200 Da ceramic membrane and of 49% for the polymeric membranes. The pore radius calculations for the NF membranes led to bigger calculated membrane pore sizes than those mentioned by the manufacturer, while a fouling assessment indicated that the tubular polymeric NF membranes are more prone to fouling than the ceramic membranes.

During the VMD experiments, the complete rejection of C5/C6 sugar and salt corroborated with literature findings regarding the performance of the MD membranes. The maximum CF of C5/C6 sugars that was achieved during the concentration experiments was 8, with a negligible permeation of sugars in the permeate side (<1%). Based on the surface tension measurements for the hydrolysate solution at different CFs and the calculated SFE of the PTFE membrane, no membrane wetting was expected for the tested membrane. However, the presence of colored droplets on the permeate side revealed a decreased hydrophobicity in different parts of the active surface area of the membrane. The contact angle measurements of synthetic sugar and NaCl solutions at different CFs showed that the wetting threshold of 90^o was not violated. However, as far as the hydrolysate solution is concerned, in the CF range of 2-5, contact angles below 90^o were measured. A combination of bigger pore sizes in the MD membrane and lower contact angles can decrease the LEP value and might have led to the partial membrane wetting observed. The fouling assessment of the MD membrane showed that there was a 50% reduction in the permeate flux after 39 hours of operation with the real hydrolysate solution. After the CIP, the membrane and the water flux were completely restored, proving that the fouling in the MD membranes is reversible. However, the fouling of the MD membranes could be a problem for full-scale applications as evinced by the frequent CIP requirements. Finally, an energy assessment of the VMD operation showed that the cooler was the most energy intensive component during the VMD operation, constituting 96% of the total energy consumption. Overall, the energy consumption of the VMD was found to be 200 KWh/ m^3 of permeate, according to the industrial scenario and 740 KWh/ m^3 of permeate, without considering a certain efficiency for the cooler (lab-scale scenario). The cooler's efficiency was, therefore, proven to be crucial in the overall energy consumption of the VMD unit. A comparison between the energy consumption of VMD and evaporators showed that the VMD is more energy efficient in comparison with evaporators with up to three effects. With the addition of more effects in the evaporators, VMD constitutes a competitive technology.

5 CONCLUSIONS

Tubular ceramic and polymeric NF and MD membranes were tested with the purpose of concentrating C5/C6 sugars amongst sugar degradation products and salt. According to the rejection values of the NF membranes, the highest C5/C6 sugar rejection of 81% was achieved with the AFC30 polymeric NF membrane. The highest C5/C6 sugar rejection value for the ceramic NF membranes was around 50% for the tightest 200 Da membrane. From the NF results, it was observed that the C5/C6 sugar rejection in the case of the hydrolysate solution was higher than the C5/C6 sugar rejection of the synthetic solutions. This difference can be explained by the presence of the sugar degradation products and organic foulants in the real hydrolysate water. The adsorption of fouling agents on the membrane pores might have led to a decreased membrane pore size and hence, to an increased rejection of the C5/C6 sugars. In terms of cleaning and fouling, the ceramic membranes performed better with a negligible decrease in the water flux after chemical cleaning. In the case of polymeric membranes, the biggest flux decrease was found to be 34 % after 4 hours of operation with the hydrolysate solution. The calculated pore sizes of the NF membranes explained the low C5/C6 sugar rejection of the different NF membranes. It was observed that the calculated membrane pore size was higher than that mentioned by the manufacturer. This finding can be seen in the case of the 450Da ceramic membrane, for which the manufacturer mentioned a pore size of 0.9 nm and the calculations have led to an average pore size of 2.2 nm. According to the NF results, it was concluded that the NF membranes were not suitable for concentrating the C5/C6 sugars due to the low sugar rejection values that were achieved.

On the contrary, experiments with the 0.2 μm MD membrane have shown > 99 % of sugar rejection independently of the feed water temperature. The sugar concentration experiment with the synthetic solution showed positive results regarding the C5/C6 sugar concentration with the VMD, by achieving a sugar CF of 8 with a negligible permeation of sugars (< 1 %). In the sugar concentration experiment with the hydrolysate water, a CF larger than 7 was achieved, where no sugars were detected in the distillate. The water flux in both experiments followed the same decreasing trend along with the increasing solute concentration. The detection of sugars in the distillate during the synthetic sugar concentration experiment and the absence of sugars in the distillate after the treatment of the hydrolysate solution led to further investigation of the membrane wetting phenomena. The contact angles of the synthetic solutions were found to be larger than 90 ^{o}, showing that the MD membrane was not susceptible to wetting with these solutions. In the case of the hydrolysate water, the contact angles in the CF range of 2-5 showed values lower than 90 ^{o} and hence, membrane wetting was expected. However, the surface tension measurements of the hydrolysate liquid at different CFs revealed high surface tension values and when compared with the calculated SFE of the membrane, no wetting phenomena were expected. Bigger pore sizes in the MD membrane and lower contact angles can lead to partial membrane wetting, as both can lead to a decreased LEP value. Consequently, the feed water is more likely to penetrate the membrane pores. According to the fluctuation in the contact angle measurements, it was deduced that the active surface area of the MD membrane was not equally hydrophobic.

Overall, it was concluded that the VMD is a suitable technology for the concentration of C5/C6 sugars, achieving partial removal of the by-products as well. This conclusion was also supported by the complete flux recovery and restoration of the membrane after 39 hours of operation and chemical cleaning. However, a frequent CIP for the MD

membrane might constitute a problem in industrial applications. The VMD technology was also assessed based on its energy efficiency to investigate if it is a feasible option in comparison with the conventional evaporation technologies. It was found that the energy consumption of the current VMD set-up was 0.22 KWh/kg distillate when taking into account the efficiency of the cooler. Comparing this value with the energy consumption of different evaporators, it can be seen that the VMD is less energy intensive when compared to evaporators with up to three effects. In the case of evaporators with more than three effects, the VMD is a competitive technology for concentrating the C5/C6 sugars. More specifically, literature values in the range of 0.12-0.18 KWh/kg condensate for 5 and 6 effect evaporators, respectively, were proven less energy intensive than the current VMD set-up. However, the capital costs in the case of multiple effect evaporators are increasing along with the addition of more effects and thus, it is not be possible to assess whether the choice of a multiple effect evaporator over a VMD unit would be more feasible. A techno-economical research is therefore necessary to conclude on which technology would be preferable in an industrial scale application.

Reflecting on the research goals of the current MSc thesis, the following research questions can be now answered:

1. How does an increase in the driving force of the tubular NF influence the rejection of the C5/C6 sugars and the permeation of salt and water?

   With an increase in the applied pressure, the rejection of the C5/C6 sugars and salt was increased as well. The highest sugar and salt rejection values were found for 50 LMH of permeate flux. The permeation of water was also increased with an increasing pressure for all solution types.

2. How does an increase in the driving force of the VMD influence the rejection of the C5/C6 sugars and salt and the permeation of water?

   The increase in the feed temperature led to a water flux increase during the VMD operation. On the contrary, the increase in the feed temperature had no effect on the rejection of the C5/C6 sugars and salt in the case of the synthetic solution. Both rejection values were larger than 99 % independently of the feed temperature. In the case of the real hydrolysate water, the increase in the feed temperature enhanced the permeation of the volatile by-products. However, the rejection of C5/C6 sugars and salt remained larger than 99% in this case as well.

3. Among tubular ceramic and polymeric NF membranes, which membrane material facilitates the concentration of the C5/C6 sugars?

   The rejection of C5/C6 sugars was higher in the case of polymeric membranes as a result of their tighter membrane pores. However, the tubular polymeric membranes proved to be more susceptible to fouling than the ceramic membranes, as a result of their final decreased MTC values.

4. Is a 10 % wt concentration of C5/C6 sugars feasible with the most suitable membrane technology?

   Concentrating the C5/C6 sugars was only possible with the VMD as a result of the complete sugar rejection from the MD membrane. The maximum CF that was achieved for the C5/C6 sugars was about 8 for both synthetic and hydrolysate solutions. The results derived from the concentration experiments with VMD indicate that water recovery values above 90% and thus a C5/C6 sugar concentration of 10 wt %, is feasible with this technology. The water flux decreased almost 50 % after the water recovery value of 80 %. However, the process of concentrating the C5/C6 sugars was still possible. Additionally, the fouling of the MD membranes was found

to be reversible after the chemical cleaning and the flux was completely recovered, hence indicating that it is possible for the sugars to reach the concentration of 10 wt % and for the membrane to be completely restored afterwards. In the case of NF, the low sugar rejection values would result in lower concentration factors, hence the NF technology was judged as unsuitable to meet the goals of the current research.

5. What is the energy consumption of the most suitable technology for concentrating the C5/C6 sugars?

   The energy consumption was calculated only in the case of VMD as it was proven to be the most appropriate technology that can meet the research goals of the current study. It was found that the VMD can be a competitive technology when compared with contemporary multi-effect evaporators in the sugar industry. With an energy consumption of 0.22 KWh/kg distillate, VMD is proven to be more energy efficient in comparison with evaporators with up to three effects. However, the energy consumption of the VMD was found to be highly affected by the cooler's efficiency and was also found to be much higher than the energy consumption reported for other pressure driven membrane processes.

6 LIMITATIONS AND RECOMMENDATIONS

The current research on the concentration of C5/C6 sugars was conducted based on laboratory set-ups and analysis with various equipment. Therefore, it is important to mention the limitations of the current study and to propose potential treatment schemes for further research.

6.1 LIMITATIONS

To assess the energy efficiency of VMD, assumptions based on the cooler's efficiency were made. The VMD set-up consisted of two gas scrub bottles that were immersed in an ice bath. In an industrial VMD application, an industrial cooler will be provided for this purpose. The COP of the cooler was roughly estimated by adopting literature values. However, a more efficient cooler would result in significantly lower energy consumption. The energy consumption of the VMD was roughly calculated based on an assumption for the cooler's efficiency and without taking into account a process integration in an industrial line. For the energy calculations, it was also assumed that the temperature of the water vapor will remain the same as in the feed water and stable at 50 ^{o} C. A small decrease in the temperature of water vapor is expected. Besides, the integration of VMD with the background process in Avantium's industrial line could result in substantial energy savings. Therefore, the calculated energy consumption needs to be interpreted with caution and to be supported with values taken from pilot installations to have a solid conclusion on the energy efficiency of VMD .

The contact angle measurements that were conducted for the investigation of the MD membrane properties, depend on the software's image processing and the baseline of the measurement. The baseline plays an important role as it can lead to e.g. $\pm$ 10 ^{o} error in contact angle measurements with a baseline shift of $\pm$ 1 pixel Chang et al. [2020]. Furthermore, the pressure gauge installed in the feed side of the VMD set-up was fluctuating throughout the whole concentration experiment, ranging from 0.1-0.5 bar due to the pulsing of the peristaltic feed pump that was used. A maximum LEP value of 0.5 bar was used for the MD calculations.

In the PHREEQC modelling used for the MTC calculation of the MD membrane, the influence of by-products in the calculation of the feed vapor pressure was not taken into account. The results of the HPLC analysis, provided by Avantium, regarding the transport of the volatile by-products in the permeate side, showed different patterns for the transport of by-products among the different VMD experiments. Due to the low by-products concentration in the feed composition, their influence in the feed vapor pressure calculations was considered as negligible.

Regarding the NF experiments, the MWCO of the membranes was only given in the case of ceramic membranes. For the membrane pore size calculations, literature values and theoretical models have been used. The average pore size was calculated by fitting the theoretical calculated solute rejection to the experimental data. Although the pore size calculations offered an insight into the pore size of the different NF membranes tested, an additional graphical estimation of the MWCO of the membranes by testing the rejection of polyethylene glycol (PEG) molecules with different MW would offer a higher

accuracy in the pore radius results. Therefore, the methodological decision that was followed in the current study may have led to an overestimation of the pore size in the NF membranes. However, the current study aimed to explain the experimentally determined sugar rejection of the different tubular NF membranes. A more in-depth and precise investigation of the properties of the different NF membranes was out of scope for the current MSc thesis.

6.2 RECOMMENDATIONS FOR FURTHER RESEARCH

Despite the suitability of the VMD for concentrating the C5/C6 sugars from the hydrolysate stream, the energy consumption of the VMD was high in comparison with other pressure-driven membrane technologies. Therefore, different membrane technologies or a combination of membrane technologies could be used to make the process of concentrating sugars more energy efficient. Since the tubular NF membranes did not meet the sugar rejection requirements, tighter membranes are proposed. RO membranes are the tightest membranes than can be used after the NF membranes. However, the presence of salt due to the stream's neutralization, is a limiting factor for the operation of an RO unit. Therefore, a pre-treatment step for desalination or de-acidification of the hydrolysate water is necessary before the concentration step with RO.

Electrodialysis (ED), which is an electrical driven membrane technology, was tested to investigate whether the hydrolysate stream can be de-acidified and desalinated. Both desalination and de-acidification experiments with ED showed promising results, with 90% removal of salt and acid and negligible sugar loss. Therefore, the addition of chemicals for the neutralization of the hydrolysate solution can be prevented in the future and the feed water can be treated afterwards with an RO unit. For the concentration step with the RO membranes, a tubular configuration is suggested. Given the previous unsuccessful attempts for concentrating the hydrolysate solution with flat-sheet membranes, a flat sheet configuration for RO would not be suggested for the concentration of the hydrolysate solution.

Additionally, the color removal (see Appendix B.2, Figure B.2) and the high sugar permeation achieved with the ceramic 450 Da membrane could be used as a pre-treatment step for the feed water entering the VMD unit. In terms of energy consumption, the energy consumption of the cooler seems to play the most important role. Therefore, a pre-treatment of the hydrolysate water is not expected to have a major impact on the energy consumption of the VMD unit. However, the flux using a pre-treated feed water would be increased due to less by-products concentration in the feed water, leading also to a reduction in the total time required for dewatering the hydrolysate solution. Additionally, the concentrate solution would be more pure as less by-products would be expected in the concentrate. In terms of fouling, using the 450 Da ceramic NF membrane as pre-treatment would result in the removal of the big fouling agents that might have enhanced the wetting phenomena on the MD membrane. Although the fouling of the MD membrane was reversible, the need for frequent chemical cleaning could be a problem in full-scale applications. The pre-treatment of the hydrolysate solution with the 450Da ceramic membrane is also proposed before the treatment scheme with the ED and tubular RO, to prevent the fouling of the RO membranes.

Overall, it can be said that the process of concentrating C5/C6 sugars with a membrane technology can be assessed based on two different factors: (i) the performance of the membrane technology regarding the maximum sugar concentration factor that can be achieved and (ii) the energy consumption of the membrane technology. If the membrane meets the performance requirements, the next step is the energy optimisation of the process. Therefore, all proposed treatment schemes need to achieve the sugar concentration

goals and to be investigated for their energy consumption and their potential integration in Avantium's background and downstream processes.

BIBLIOGRAPHY

A Shirazi, M. M. and Kargari, A. (2019). Concentrating of sugar syrup in bioethanol production using sweeping gas membrane distillation. *Membranes*, 9(5):59.

Abu-Zeid, M. A. E.-R., Zhang, Y., Dong, H., Zhang, L., Chen, H.-L., and Hou, L. (2015). A comprehensive review of vacuum membrane distillation technique. *Desalination*, 356:1–14.

Ajao, O., Rahni, M., Marinova, M., Chadjaa, H., and Savadogo, O. (2017). Study of separation and fouling of reverse osmosis membranes during model hydrolysate solution filtration. *Membranes*, 7(4):68.

Al-Asheh, S., Banat, F., Qtaishat, M., and Al-Khateeb, M. (2006). Concentration of sucrose solutions via vacuum membrane distillation. *Desalination*, 195(1-3):60–68.

Alkhudhiri, A., Darwish, N., and Hilal, N. (2012). Membrane distillation: A comprehensive review. *Desalination*, 287:2–18.

Allen, A. L. (2009). Efficiency and performance measurements of a pdc inc. single stage diaphragm hydrogen compressor.

Amidon, T. E. and Liu, S. (2009). Water-based woody biorefinery. *Biotechnology advances*, 27(5):542–550.

Amjad, Z. (1993). *Reverse osmosis: membrane technology, water chemistry, and industrial applications*. Van Nostrand Reinhold New York.

Árki, P., Hecker, C., Tomandl, G., and Joseph, Y. (2019). Streaming potential properties of ceramic nanofiltration membranes–importance of surface charge on the ion rejection. *Separation and Purification Technology*, 212:660–669.

Bannwarth, H. (2005). Liquid ring vacuum pumps, compressors and systems: Conventional and hermetic design.

Bargeman, G., Westerink, J., Miguez, O. G., and Wessling, M. (2014). The effect of nacl and glucose concentration on retentions for nanofiltration membranes processing concentrated solutions. *Separation and purification technology*, 134:46–57.

Bellona, C., Marts, M., and Drewes, J. E. (2010). The effect of organic membrane fouling on the properties and rejection characteristics of nanofiltration membranes. *Separation and Purification Technology*, 74(1):44–54.

Bi, F., Zhao, H., Zhang, L., Ye, Q., Chen, H., and Gao, C. (2014). Discussion on calculation of maximum water recovery in nanofiltration system. *Desalination*, 332(1):142–146.

Bouchoux, A., Roux-de Balmann, H., and Lutin, F. (2005). Nanofiltration of glucose and sodium lactate solutions: Variations of retention between single-and mixed-solute solutions. *Journal of membrane science*, 258(1-2):123–132.

Bouranene, S., Szymczyk, A., Fievet, P., and Vidonne, A. (2009). Effect of salts on the retention of polyethyleneglycol by a nanofiltration ceramic membrane. *Desalination*, 240(1-3):94–98.

Bowen, W. R. and Welfoot, J. S. (2002). Modelling the performance of membrane nanofiltration—critical assessment and model development. *Chemical engineering science*, 57(7):1121–1137.

Brodin, M., Vallejos, M., Opedal, M. T., Area, M. C., and Chinga-Carrasco, G. (2017). Lignocellulosics as sustainable resources for production of bioplastics–a review. *Journal of Cleaner Production*, 162:646–664.

Bush, J. A., Vanneste, J., and Cath, T. Y. (2016). Membrane distillation for concentration of hypersaline brines from the great salt lake: Effects of scaling and fouling on performance, efficiency, and salt rejection. *Separation and Purification Technology*, 170:78–91.

Caltran, I., Rietveld, L., Shorney-Darby, H., and Heijman, S. (2020). Separating nom from salts in ion exchange brine with ceramic nanofiltration. *Water Research*, page 115894.

Chang, H., Liu, B., Zhang, Z., Pawar, R., Yan, Z., Crittenden, J. C., and Vidic, R. D. (2020). A critical review of membrane wettability in membrane distillation from the perspective of interfacial interactions. *Environmental Science & Technology*.

Chen, J., Zhang, Y., Wang, Y., Ji, X., Zhang, L., Mi, X., and Huang, H. (2013). Removal of inhibitors from lignocellulosic hydrolyzates by vacuum membrane distillation. *Bioresource technology*, 144:680–683.

Chiam, C.-K. and Sarbatly, R. (2013). Vacuum membrane distillation processes for aqueous solution treatment—a review. *Chemical Engineering and Processing: Process Intensification*, 74:27–54.

Chong, J. Y. and Wang, R. (2019). From micro to nano: Polyamide thin film on microfiltration ceramic tubular membranes for nanofiltration. *Journal of Membrane Science*, 587:117161.

Christopher, L. (2012). Adding value prior to pulping: bioproducts from hemicellulose. *Global perspectives on sustainable forest management. New York: Tech*, pages 225–46.

Clark, S. M. and Konermann, L. (2004). Screening for noncovalent ligand- receptor interactions by electrospray ionization mass spectrometry-based diffusion measurements. *Analytical chemistry*, 76(5):1257–1263.

Criscuoli, A., Carnevale, M. C., and Drioli, E. (2008). Evaluation of energy requirements in membrane distillation. *Chemical Engineering and Processing: Process Intensification*, 47(7):1098–1105.

Da Costa, A., Fane, A., and Wiley, D. (1994). Spacer characterization and pressure drop modelling in spacer-filled channels for ultrafiltration. *Journal of membrane science*, 87(1-2):79–98.

da Silva Pereira, G., Primo, A. R., and Villa, A. A. O. (2015). < b> comparative study of air conditioning systems with vapor compression chillers using the concept of green buildings. *Acta Scientiarum. Technology*, 37(4):339–346.

De Bhowmick, G., Sarmah, A. K., and Sen, R. (2018). Lignocellulosic biorefinery as a model for sustainable development of biofuels and value added products. *Bioresource technology*, 247:1144–1154.

Dechadilok, P. and Deen, W. M. (2006). Hindrance factors for diffusion and convection in pores. *Industrial & Engineering Chemistry Research*, 45(21):6953–6959.

Dey, P., Pal, P., Kevin, J. D., and Das, D. B. (2020). Lignocellulosic bioethanol production: prospects of emerging membrane technologies to improve the process–a critical review. *Reviews in Chemical Engineering*, 36(3):333–367.

Doherty, W. O., Rackemann, D. W., and Steindl, R. J. (2010). Fouling of tubular ceramic membranes during processing of cane sugar juice. *Desalination and Water Treatment*, 16(1-3):45–56.

Duong, H. C., Cooper, P., Nelemans, B., Cath, T. Y., and Nghiem, L. D. (2016). Evaluating energy consumption of air gap membrane distillation for seawater desalination at pilot scale level. *Separation and Purification Technology*, 166:55–62.

El-Bourawi, M., Ding, Z., Ma, R., and Khayet, M. (2006). A framework for better understanding membrane distillation separation process. *Journal of membrane science*, 285(1-2):4–29.

Eykens, L., De Sitter, K., Dotremont, C., De Schepper, W., Pinoy, L., and Van Der Bruggen, B. (2017). Wetting resistance of commercial membrane distillation membranes in waste streams containing surfactants and oil. *Applied Sciences*, 7(2):118.

Franken, A., Nolten, J., Mulder, M., Bargeman, D., and Smolders, C. (1987). Wetting criteria for the applicability of membrane distillation. *Journal of Membrane Science*, 33(3):315–328.

Galbe, M. and Wallberg, O. (2019). Pretreatment for biorefineries: a review of common methods for efficient utilisation of lignocellulosic materials. *Biotechnology for Biofuels*, 12(1):1–26.

García-Payo, M. d. C., Izquierdo-Gil, M. A., and Fernández-Pineda, C. (2000). Wetting study of hydrophobic membranes via liquid entry pressure measurements with aqueous alcohol solutions. *Journal of colloid and interface science*, 230(2):420–431.

Gautam, A. and Menkhaus, T. J. (2014). Performance evaluation and fouling analysis for reverse osmosis and nanofiltration membranes during processing of lignocellulosic biomass hydrolysate. *Journal of Membrane Science*, 451:252–265.

Ghazali, N. F. and Razak, N. D. A. (2021). Recovery of saccharides from lignocellulosic hydrolysates using nanofiltration membranes: A review. *Food and Bioproducts Processing*.

Guo, S., Luo, J., Yang, Q., Qiang, X., Feng, S., and Wan, Y. (2019). Decoloration of molasses by ultrafiltration and nanofiltration: unraveling the mechanisms of high sucrose retention. *Food and Bioprocess Technology*, 12(1):39–53.

Hasan, A., Yasarla, R., Ramarao, B., and Amidon, T. (2011). Separation of lignocellulosic hydrolyzate components using ceramic microfilters. *Journal of wood chemistry and technology*, 31(4):357–383.

Hinkova, A., Bubnık, Z., Kadlec, P., and Pridal, J. (2002). Potentials of separation membranes in the sugar industry. *Separation and Purification Technology*, 26(1):101–110.

Humpert, D., Ebrahimi, M., and Czermak, P. (2016). Membrane technology for the recovery of lignin: A review. *Membranes*, 6(3):42.

Huttunen, M., Nygren, L., Kinnarinen, T., Häkkinen, A., Lindh, T., Ahola, J., and Karvonen, V. (2017). Specific energy consumption of cake dewatering with vacuum filters. *Minerals Engineering*, 100:144–154.

Intan Shafinas Muhammad, N. and A Rosentrater, K. (2020). Economic assessment of bioethanol recovery using membrane distillation for food waste fermentation. *Bioengineering*, 7(1):15.

Jenkins, R. and Bell, R. (1987). Molecular radii of probes used in studies of intestinal permeability. *Gut*, 28(1):110.

Jiao, B., Cassano, A., and Drioli, E. (2004). Recent advances on membrane processes for the concentration of fruit juices: a review. *Journal of food engineering*, 63(3):303–324.

Käldström, M., Meine, N., Farès, C., Rinaldi, R., and Schüth, F. (2014). Fractionation of 'water-soluble lignocellulose'into c 5/c 6 sugars and sulfur-free lignins. *Green Chemistry*, 16(5):2454–2462.

Kozbial, A., Li, Z., Conaway, C., McGinley, R., Dhingra, S., Vahdat, V., Zhou, F., D'Urso, B., Liu, H., and Li, L. (2014). Study on the surface energy of graphene by contact angle measurements. *Langmuir*, 30(28):8598–8606.

Kucera, J. (2019). *Desalination: water from water*. John Wiley & Sons.

Labban, O., Liu, C., Chong, T. H., et al. (2017). Fundamentals of low-pressure nanofiltration: Membrane characterization, modeling, and understanding the multi-ionic interactions in water softening. *Journal of Membrane Science*, 521:18–32.

Li, L. and Sirkar, K. K. (2017). Studies in vacuum membrane distillation with flat membranes. *Journal of Membrane Science*, 523:225–234.

Lide, D. R. (2004). *CRC handbook of chemistry and physics*, volume 85. CRC press.

Liu, J., Qin, Y., Li, P., Zhang, K., Liu, Q., and Liu, L. (2016). Separation of the acid-sugar mixtures by using acid retardation and further concentration of the eluents by using continuous-effect membrane distillation. *Journal of Chemical Technology & Biotechnology*, 91(4):1105–1112.

Luo, J. and Wan, Y. (2011). Effect of highly concentrated salt on retention of organic solutes by nanofiltration polymeric membranes. *Journal of membrane science*, 372(1-2):145–153.

Luo, J. and Wan, Y. (2013). Effects of ph and salt on nanofiltration—a critical review. *Journal of membrane Science*, 438:18–28.

Madaeni, S. and Zereshki, S. (2008). Reverse osmosis alternative: Energy implication for sugar industry. *Chemical Engineering and Processing: Process Intensification*, 47(7):1075–1080.

Madhumala, M., Madhavi, D., Sankarshana, T., and Sridhar, S. (2014). Recovery of hydrochloric acid and glycerol from aqueous solutions in chloralkali and chemical process industries by membrane distillation technique. *Journal of the Taiwan Institute of Chemical Engineers*, 45(4):1249–1259.

Magalhaes, H. L. F., de Lima, A. G. B., de Farias Neto, S. R., Alves, H. G., and de Souza, J. S. (2017). Produced water treatment by ceramic membrane: A numerical investigation by computational fluid dynamics. *Advances in Mechanical Engineering*, 9(3):1687814016688642.

Maiti, S. K., Thuyavan, Y. L., Singh, S., Oberoi, H. S., and Agarwal, G. P. (2012). Modeling of the separation of inhibitory components from pretreated rice straw hydrolysate by nanofiltration membranes. *Bioresource technology*, 114:419–427.

Malmali, M., Stickel, J. J., and Wickramasinghe, S. R. (2014). Sugar concentration and detoxification of clarified biomass hydrolysate by nanofiltration. *Separation and Purification Technology*, 132:655–665.

Meng, X. and Ragauskas, A. J. (2017). Pseudo-lignin formation during dilute acid pretreatment for cellulosic ethanol. *Recent Advances in Petrochemical Science*, 1(1).

Mengual, J., Khayet, M., and Godino, M. (2004). Heat and mass transfer in vacuum membrane distillation. *International Journal of Heat and Mass Transfer*, 47(4):865–875.

Micari, M., Diamantidou, D., Heijman, B., Moser, M., Haidari, A., Spanjers, H., and Bertsch, V. (2020). Experimental and theoretical characterization of commercial nanofiltration membranes for the treatment of ion exchange spent regenerant. *Journal of Membrane Science*, 606:118117.

Mohammad, A. W. (2002). A modified donnan–steric-pore model for predicting flux and rejection of dye/nacl mixture in nanofiltration membranes. *Separation Science and Technology*, 37(5):1009–1029.

Mohammad, A. W., Basha, R. K., and Leo, C. P. (2010). Nanofiltration of glucose solution containing salts: Effects of membrane characteristics, organic component and salts on retention. *Journal of food engineering*, 97(4):510–518.

Mojab, S., Pollard, A., Pharoah, J. G., Beale, S. B., and Hanff, E. S. (2014). Unsteady laminar to turbulent flow in a spacer-filled channel. *Flow, turbulence and combustion*, 92(1-2):563–577.

Murthy, G., Sridhar, S., Sunder, M. S., Shankaraiah, B., and Ramakrishna, M. (2005). Concentration of xylose reaction liquor by nanofiltration for the production of xylitol sugar alcohol. *Separation and purification technology*, 44(3):221–228.

Nene, S., Kaur, S., Sumod, K., Joshi, B., and Raghavarao, K. (2002). Membrane distillation for the concentration of raw cane-sugar syrup and membrane clarified sugarcane juice. *Desalination*, 147(1-3):157–160.

Oatley, D. L., Llenas, L., Aljohani, N. H., Williams, P. M., Martínez-Lladó, X., Rovira, M., and de Pablo, J. (2013). Investigation of the dielectric properties of nanofiltration membranes. *Desalination*, 315:100–106.

Oliveira, C. R. (2018). Separation of sugars by ceramic nanofiltration membranes.

Oriez, V., Peydecastaing, J., and Pontalier, P.-Y. (2020). Lignocellulosic biomass mild alkaline fractionation and resulting extract purification processes: conditions, yields, and purities. *Clean Technologies*, 2(1):91–115.

Parkhurst, D. L. and Appelo, C. (2013). Description of input and examples for phreeqc version 3: a computer program for speciation, batch-reaction, one-dimensional transport, and inverse geochemical calculations. Technical report, US Geological Survey.

Peng, X., Nie, S., Li, X., Huang, X., and Li, Q. (2019). Characteristics of the water-and alkali-soluble hemicelluloses fractionated by sequential acidification and graded-ethanol from sweet maize stems. *Molecules*, 24(1):212.

Politano, A., Di Profio, G., Fontananova, E., Sanna, V., Cupolillo, A., and Curcio, E. (2019). Overcoming temperature polarization in membrane distillation by thermoplasmonic effects activated by ag nanofillers in polymeric membranes. *Desalination*, 451:192–199.

Prado, C., Souza, O., Sellin, N., and Marangoni, C. (2015). Comparison between single and multi-effect evaporators for sugar concentration in ethanol production. *chemical engineering transactions*, 43:541–546.

Rafik, M., Qabli, H., Belhamidi, S., Elhannouni, F., Elkhedmaoui, A., and Elmidaoui, A. (2015). Membrane separation in the sugar industry. *Journal of Chemical and Pharmaceutical Research*, 7(9):653–658.

Reynolds, O. (1883). Xxix. an experimental investigation of the circumstances which determine whether the motion of water shall be direct or sinuous, and of the law of resistance in parallel channels. *Philosophical Transactions of the Royal society of London*, (174):935–982.

Roli, N., Yussof, H., Seman, M., Saufi, S., and Mohammad, A. W. (2016). Separating xylose from glucose using spiral wound nanofiltration membrane: effect of cross-flow parameters on sugar rejection. In *IOP conference series: materials science and engineering*, volume 162, page 012035. IOP Publishing.

Roy, S. and Ragunath, S. (2018). Emerging membrane technologies for water and energy sustainability: Future prospects, constraints and challenges. *Energies*, 11(11):2997.

Samee, M. A., Elgohary, A. A., Harasek, M., and Friedl, A. (2016). Experimental investigation of nanofiltration process for the separation of complex sugar mixtures containing mono-and multivalent salts. *Chemical Engineering Transactions*, 52:799–804.

Sarma, G. and Barma, S. D. (2010). Energy management in multiple–effect evaporator system: A heat balance analysis approach. *Gen*, 1(2):84–88.

Schock, G. and Miquel, A. (1987). Mass transfer and pressure loss in spiral wound modules. *Desalination*, 64:339–352.

Schuck, P., Jeantet, R., Tanguy, G., Méjean, S., Gac, A., Lefebvre, T., Labussière, E., and Martineau, C. (2015). Energy consumption in the processing of dairy and feed powders by evaporation and drying. *Drying Technology*, 33(2):176–184.

Shaker, M. and Salahinejad, E. (2018). A combined criterion of surface free energy and roughness to predict the wettability of non-ideal low-energy surfaces. *Progress in Organic Coatings*, 119:123–126.

Sharan, P. and Bandyopadhyay, S. (2016). Energy integration of multiple effect evaporators with background process and appropriate temperature selection. *Industrial & Engineering Chemistry Research*, 55(6):1630–1641.

Shirley, J., Mandale, S., and Kochkodan, V. (2014). Influence of solute concentration and dipole moment on the retention of uncharged molecules with nanofiltration. *Desalination*, 344:116–122.

Sinha Ray, S., Lee, H.-K., and Kwon, Y.-N. (2020). Review on blueprint of designing anti-wetting polymeric membrane surfaces for enhanced membrane distillation performance. *Polymers*, 12(1):23.

Sjölin, M., Thuvander, J., Wallberg, O., and Lipnizki, F. (2020). Purification of sucrose in sugar beet molasses by utilizing ceramic nanofiltration and ultrafiltration membranes. *Membranes*, 10(1):5.

Steinbach, D., Kruse, A., and Sauer, J. (2017). Pretreatment technologies of lignocellulosic biomass in water in view of furfural and 5-hydroxymethylfurfural production-a review. *Biomass Conversion and Biorefinery*, 7(2):247–274.

Su, P. (2012). Sorption of metal ions to wood, pulp and bark materials.

Sundergopal, S., Moulik, S., and Nagar, H. (2015). Membranes for solvent dewatering.

Tokareva, E. N., Pranovich, A. V., Fardim, P., Daniel, G., and Holmbom, B. (2007). Analysis of wood tissues by time-of-flight secondary ion mass spectrometry.

Trägårdh, G. and Gekas, V. (1988). Membrane technology in the sugar industry. *Desalination*, 69(1):9–17.

Ullah, R., Khraisheh, M., Esteves, R. J., McLeskey Jr, J. T., AlGhouti, M., Gad-el Hak, M., and Tafreshi, H. V. (2018). Energy efficiency of direct contact membrane distillation. *Desalination*, 433:56–67.

Valentas, K. J., Rotstein, E., and Singh, R. P. (1997). *Handbook of food engineering practice*. CRC press.

Van Zandvoort, I. (2015). *Towards the valorization of humin by-products: characterization, solubilization and catalysis*. PhD thesis, University Utrecht.

Vellenga, E. and Trägårdh, G. (1998). Nanofiltration of combined salt and sugar solutions: coupling between retentions. *Desalination*, 120(3):211–220.

Verissimo, S., Peinemann, K.-V., and Bordado, J. (2005). New composite hollow fiber membrane for nanofiltration. *Desalination*, 184(1-3):1–11.

Vestfálová, M. and Šafařík, P. (2016). Dependence of the isobaric specific heat capacity of water vapor on the pressure and temperature. In *EPJ Web of Conferences*, volume 114, page 02133. EDP Sciences.

Wagner, W. and Pruß, A. (2002). The iapws formulation 1995 for the thermodynamic properties of ordinary water substance for general and scientific use. *Journal of physical and chemical reference data*, 31(2):387–535.

Wang, Z., Winestrand, S., Gillgren, T., and Jönsson, L. J. (2018). Chemical and structural factors influencing enzymatic saccharification of wood from aspen, birch and spruce. *Biomass and Bioenergy*, 109:125–134.

Xie, Z., Ng, D., Hoang, M., Adnan, S., Zhang, J., Duke, M., Li, J.-D., Groth, A., Tun, C., and Gray, S. (2016). Preliminary evaluation for vacuum membrane distillation (vmd) energy requirement. *Journal of Membrane Science and Research*, 2(4):207–213.

Ying Shi, C., Hui Ting, L. L., and Boon Seng, O. (2020). Membrane distillation for water recovery and its fouling phenomena. *Journal of Membrane Science and Research*, 6(1):107–124.

Zhang, H., Luo, J., Liu, L., Chen, X., and Wan, Y. (2020). Green production of sugar by membrane technology: How far is it from industrialization? *Green Chemical Engineering*.

Zhang, J., Duke, M., Xie, Z., Gray, S., et al. (2010). Performance of asymmetric hollow fibre membranes in membrane distillation under various configurations and vacuum enhancement. *Journal of Membrane Science*, 362(1-2):517–528.

Zhang, L., Wang, Y., Cheng, L.-H., Xu, X., and Chen, H. (2012). Concentration of lignocellulosic hydrolyzates by solar membrane distillation. *Bioresource technology*, 123:382–385.

Zhang, Y., Li, M., Wang, Y., Ji, X., Zhang, L., and Hou, L. (2015). Simultaneous concentration and detoxification of lignocellulosic hydrolyzates by vacuum membrane distillation coupled with adsorption. *Bioresource technology*, 197:276–283.

Zhang, Y., Munir, M. T., Udugama, I., Yu, W., and Young, B. R. (2018). Modelling of a milk powder falling film evaporator for predicting process trends and comparison of energy consumption. *Journal of Food Engineering*, 225:26–33.

A CALCULATIONS

A.1 MATHEMATICAL FORMULATION OF THE DSPM

The mathematical formulation of the DSPM model is given with the following Equation A.1, which was further in analysed Section 3.6, to predict the NF rejection mechanisms based on Donnan exclusion and sieving effect mechanisms [Ghazali and Razak, 2021].

$$j_s = K_{s,c} \times C_s \times J_v - \frac{C_s \times D_{s,p}}{R_g \times T} \times \frac{d_{\mu_s}}{d(x/\epsilon)} \tag{A.1}$$

where j_s and J_v are the solute and total volume fluxes across the membrane, respectively. $K_{s,c}$ is the hindrance coefficient for convection, $D_{s,p}$ is the hindered diffusivity of the solute inside the membrane pores and C_s is the concentration of the solute in membrane pores. R and T are the gas constant and the absolute temperature, respectively. The μ term is the chemical potential of the species and finally x and ϵ are the axial coordinate inside the membrane pore and the porosity of the membrane, respectively. The water flux J_v is given by the Hagen-Poiseulle formula in Equation A.2 [Micari et al., 2020].

$$J_v = \frac{\Delta P \times r_p^2}{8 \times \eta \times \delta_m} \tag{A.2}$$

where, it can be deduced that the water flux is dependant on the pore radius of the membrane (r_p), membrane thickness (δ_m), the dynamic viscosity of the solution (η) and the net pressure difference (ΔP).

A.2 HYDRAULIC CALCULATIONS FOR NF AND MD

A.2.1 Calculations for open channels

For a tubular membrane, the following formulas can be used in order to determine the fluid dynamic behaviour. The cross-sectional velocity (u_o) in the module can be given by [Reynolds, 1883]:

$$u_o = \frac{Re \times \mu_{water}}{\rho_{water} \times d_h} \tag{A.3}$$

where Re is the Reynolds number, d_h is the hydraulic diameter, ρ_{water} is the density and μ_{water} is the viscosity of water respectively. To avoid or reduce the concentration polarisation phenomena, a turbulent flow is suggested. In terms of Reynolds number, a turbulent flow can be achieved when the value of Reynolds number is larger than 2100. Equation A.3 can also be expressed based on the kinematic viscosity (v_w) as [Schock and Miquel, 1987]:

$$u_o = \frac{Re \times v_w}{d_h} \tag{A.4}$$

The kinematic viscosity, respectively, is solely dependant on the temperature as described in Equation A.5:

$$v_w = \frac{4.97 \times 10^{-4}}{T + 42.5^{1.5}} \tag{A.5}$$

For circular open channels, the hydraulic diameter can be calculated based on the following formula :

$$d_h = \frac{4 \times (1/4 \times \pi \times D_c^2)}{\pi \times D_c} \tag{A.6}$$

where, Dc is the channel diameter.

A.2.2 Calculations for spacer-filled channels

For the hydraulic calculations of a spacer filled channel, Schock and Miquel proposed the following formula for the hydraulic diameter calculation, which will be used for the calculation of hydraulic conditions:

$$d_{h,sfc} = \frac{4 \times V_c}{A_{w,t}} \tag{A.7}$$

where V_c is the flow channel volume $[m^3]$ and $A_{w,t}$ the total wetted surface area $[m^2]$. The flow channel volume can be computed from Equation A.8.

$$V_c = V_t - V_s \tag{A.8}$$

where V_t is the total volume and V_s the spacer volume, both expressed in $[m^3]$. The V_t and V_s are given in the following formulas [Da Costa et al., 1994]:

$$V_t = l_{m,1} \times l_{m,2} \times sin\theta \times h_c \tag{A.9}$$

where, θ is the orientation angle of the filament and $l_{m,i}$ the distance between the spacer filaments, given in m.

$$\begin{aligned} V_s &= 2 \times \frac{1}{2} \times (\frac{1}{4} \times \pi \times d_{f,1}^2 \times l_{m,1}) + 2 \times \frac{1}{2} (\frac{1}{4} \times \pi \times d_{f,2}^2 \times l_{m,2}) \\ &= \frac{1}{4} \times \pi \times (d_{f,1}^2 \times l_{m,1} + d_{f,2}^2 \times l_{m,2}) \end{aligned} \tag{A.10}$$

where, df_i is the diameter of the filaments. Each filament in the feed spacer is a part of two meshes and thus, half of the volume and half of the wetted surface area are taken into account. Every mesh of the feed spacer consists of four filament sides. Finally, the total wetted surface area can be given as [Da Costa et al., 1994]:

$$A_{w,t} = A_{w,fc} + A_{w,s} \tag{A.11}$$

where $A_{w,fc}$ and $A_{w,s}$ are the wetted surface area of the flow channel and of the spacer in m^2, respectively . These two terms are given in Equations A.12 & A.13, respectively.

$$A_{w,fc} = 2 \times l_{m,1} \times l_{m,2} \times sin\theta \tag{A.12}$$

$$\begin{aligned} A_{w,s} &= 2 \times \frac{1}{2} \times (\pi \times d_{f,1} \times l_{m,1}) + 2 \times \frac{1}{2} \times (\pi \times d_{f,2} \times l_{m,2}) \\ &= \pi \times (d_{f,1} \times l_{m,1} + d_{f,2} \times l_{m,2}) \end{aligned} \tag{A.13}$$

The filament of the 47 mil feed spacer can be seen in Figure A.1 as taken from the digital microscopy. Based on these measurements, the values in Table A.1 were used for the hydraulic calculation of the VMD set-up.

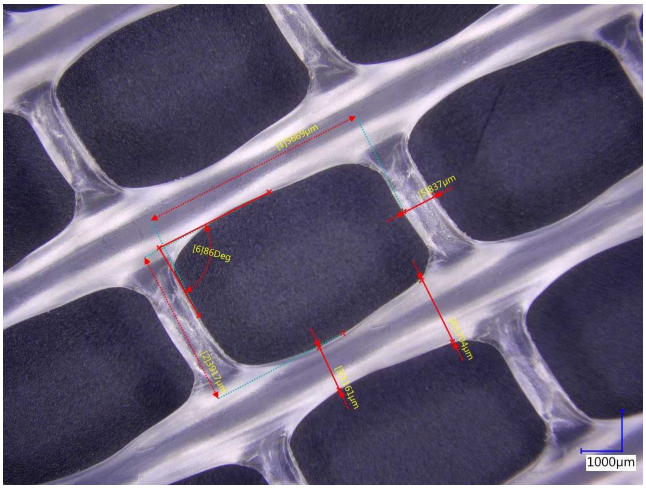

Fig. A.1: The 47 mil feed spacer provided by Sterlitech with the filament dimensions as measured with the digital microscope

Table A.1: Values of filament parameters of the 47mil feed spacer taken from digital microscopy

Parameter	Value	Unit
$d_{f,1}$	1.43E-03	m
$d_{f,2}$	8.37E-04	m
$l_{m,1}$	5.67E-03	m
$l_{m,2}$	3.92E-03	m
θ	1.50	rad

B LABORATORY ACTIVITIES

B.1 PREVIOUS NANOFILTRATION TESTS

The previous attempts for concentrating the hydrolysate solution of Avantium using a flat-sheet NF membrane with MWCO of 150 Da, can be seen in Figure B.1. After testing the hydrolate solution, fouling was observed on the NF membrane as it can be seen by the color on the surface of the membrane (Figure B.1a). Fouling was also observed in the feed spacer with the presence of black particles (Figure B.1b).

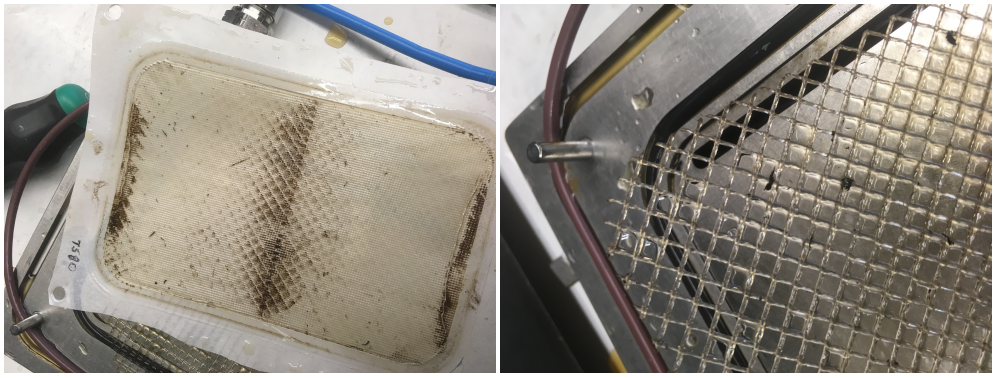

(a) Fouling of the NF membrane after testing the hydrolysate solution

(b) Spacer fouling after testing the hydrolysate solution

Fig. B.1: Fouling of the flat-sheet nanofiltration membrane and of feed spacer, during previous testing of the hydrolysate solution

B.2 COLOR REMOVAL WITH CERAMIC NF

In Figure B.2, the color removal of the hydrolysate solution with the 450Da ceramic NF membrane can be seen for different samples at different applied pressure values. It can be observed that with an increase in the driving force, the solution becomes more transparent. That can be attributed to the higher rejection of by-products with higher applied pressure values.

B.3 CONTACT ANGLE AND SURFACE TENSION MEASUREMENTS

The results of the surface tension measurements for the hydrolysate samples at different water recovery values can be seen in Table B.1. The results from the contact angle measurements of synthetic and hydrolysate solutions can be seen in Table B.2 & B.3, where $Part_I$, $Part_{II}$, $Part_{III}$ and $Part_{IV}$ are the different parts of the membrane surface area. A visual representation of the contact angles with the hydrolysate solution on the MD membrane is given in Figure B.3. Additionally, in Figures B.4 & B.5, the contact angles of the different synthetic solutions and diiodomethane on the MD membrane can be seen, respectively. In Figure B.6, the ring method for the surface tension measurements is depicted.

Fig. B.2: Decoloration of the hydrolysate solution with the 450Da ceramic NF membrane for increasing (left to right) pressure values

Table B.1: Surface tension measurements of the hydrolysate samples at different recovery values

Surface tension measurements		
Recovery	Value	Units
0 %	58.9	mN/m
66 %	62.56	mN/m
78 %	61.1	mN/m
83 %	61.64	mN/m
86 %	59.18	mN/m

Table B.2: Contact angle measurements of synthetic solutions water on three different parts of the PTFE MD membrane

Contact angle measurements (^{o})					
Solution	CF	$Part_I$	$Part_{II}$	$Part_{III}$	Average
NaCl	1	123.35	109.20	120.72	117.76
NaCl	7	100.50	113.20	121.66	111.79
NaCl+sugar mixture	1	107.38	103.33	112.17	107.63
NaCl+sugar mixture	5	113.80	125.29	97.04	112.05
NaCl+sugar mixture	7	105.73	102.64	114.10	107.49

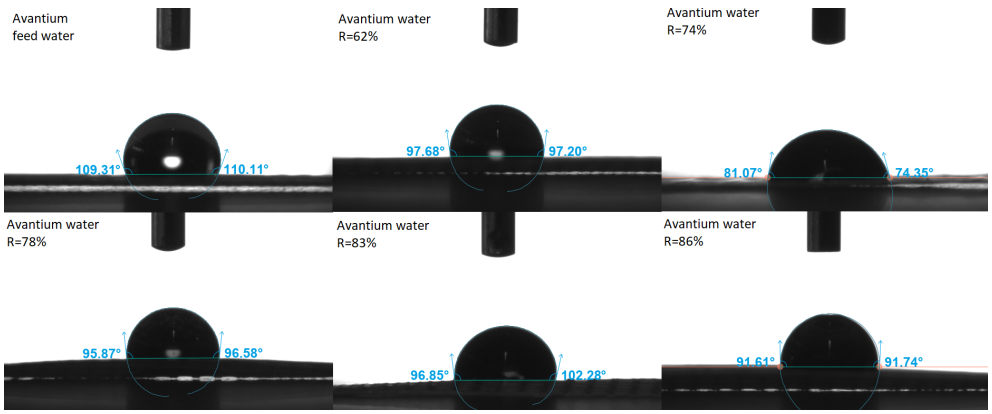

Fig. B.3: Contact angles of hydrolysate samples at different recovery values as generated by the apparatus

Table B.3: Contact angle measurements of the hydrolysate solution at different concentration factors on four different parts of the PTFE MD membrane

Contact angle measurements (^{o})						
Solution	Recovery (%)	$Part_I$	$Part_{II}$	$Part_{III}$	$Part_{IV}$	Average
AVT water	0	106.53	109.22	95.70	100.97	103.11
AVT water	51	97.91	94.59	97.97	104.02	98.62
AVT water	58	103.58	114.61	67.19	69.92	88.82
AVT water	62	127.64	106.76	97.83	111.72	110.99
AVT water	74	77.81	102.11	89.28	87.54	89.19
AVT water	78	111.58	95.76	102.44	95.02	101.20
AVT water	83	99.61	98.54	108.45	109.93	104.13
AVT water	86	118.460	102.86	93.02	94.21	102.14

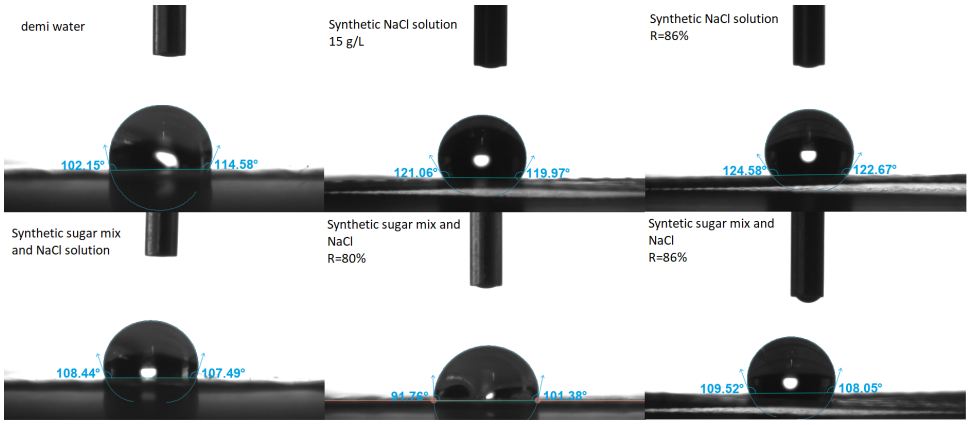

Fig. B.4: Contact angles of synthetic solutions at different recovery values as generated by the apparatus

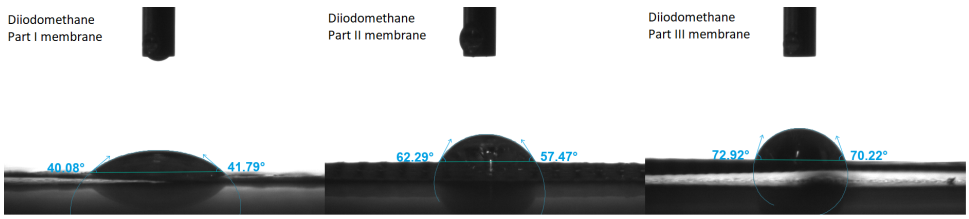

Fig. B.5: Contact angles of diiodomethane at different parts of the MD membrane as generated by the apparatus

Fig. B.6: Surface tension measurements of the hydrolysate solution with the ring method